# Joint Gaussian Graphical Model Estimation: A Survey

Katherine Tsai<sup>1</sup>, Oluwasanmi Koyejo<sup>2</sup>, and Mladen Kolar<sup>3</sup>

<sup>1</sup>Department of Electrical and Computer Engineering, University of Illinois at Urbana-Champaign

<sup>2</sup>Department of Computer Science, University of Illinois at Urbana-Champaign <sup>3</sup>Booth School of Business, The University of Chicago

October 22, 2021

### Abstract

Graphs from complex systems often share a partial underlying structure across domains while retaining individual features. Thus, identifying common structures can shed light on the underlying signal, for instance, when applied to scientific discoveries or clinical diagnoses. Furthermore, growing evidence shows that the shared structure across domains boosts the estimation power of graphs, particularly for high-dimensional data. However, building a joint estimator to extract the common structure may be more complicated than it seems, most often due to data heterogeneity across sources. This manuscript surveys recent work on statistical inference of joint Gaussian graphical models, identifying model structures that fit various data generation processes. Simulations under different data generation processes are implemented with detailed discussions on the choice of models.

### 1 Introduction

Graphical models are powerful tools for expressing statistical relationships between variables. Examples of practical use are ubiquitous, and include models that characterize the causal relationships between the neurological activity of brain regions, genetic expression across genes, and a variety of other physiological measurements. A variety of applications have illustrated the value of graphical models for analyzing scientific phenomena (Felsenstein, 1981; Schäfer and Strimmer, 2005; Friedman et al., 2000; Chan et al., 2017; Dondelinger et al., 2013). Specifically, graphical models have proven useful for elucidating the mechanisms of brain function (Foti and Fox, 2019; Manning et al., 2018; Schwab et al., 2018; Greenewald et al., 2017; Colclough et al., 2018; Qiu et al., 2016; Skripnikov and Michailidis, 2019). This manuscript outlines joint graphical models, an extension to standard graphical models that are useful for jointly analyzing data from multiple sources, e.g., neurological data measured at multiple timescales, or joint neurological, genetic and phenotypic data. Specifically, this manuscript lays out the representation of joint graphical models and some of their properties, then outlines the best practices for estimating joint graphical models. This manuscript provides examples of data generation processes where the joint approach can significantly improve estimates compared to separate estimation.

A graph G = (V, E) consists of a set of p nodes, also known as vertices  $V = \{1, \ldots, p\}$  and a set of edges  $E \subseteq V \times V$ . In a probabilistic graphical model (Lauritzen, 1996), the set of nodes V is associated with coordinates of a random vector  $\mathbf{x} = (x_1, \ldots, x_p)^{\top}$  and the edge set E captures dependency relationships between the components of the vector. In particular, in an undirected probabilistic graphical model, the absence of an edge between nodes a and b indicates that  $x_a$  and  $x_b$  are conditionally independent given all other variables  $x_{-\{a,b\}} = \{x_c \mid c \in V \setminus \{a,b\}\}$ . In a neuroscience application, the random vector  $\mathbf{x}$  could represent, for example, measurements of brain activity in different regions – so the set of edges corresponds

to functional brain connectivity. Given n measurements of the vector  $\mathbf{x}$ , inferring the graph structure corresponds to identifying pairs of coordinates that are conditionally independent given all other variables (Drton and Maathuis, 2017). Inferring the graph structure based on conditional associations is more challenging than inferring the correlation structure between the measurements. However, the conditional independence graphs are generally considered more scientifically meaningful (Dobra et al., 2004).

## 2 Background: Gaussian Graphical Models

The most widely used examples of probabilistic graphical models are Gaussian graphical models, where  $\mathbf{x} \sim \mathcal{N}(\boldsymbol{\mu}, \mathbf{\Omega}^{-1})$  is assumed to be distributed as a multivariate Gaussian vector with mean vector  $\boldsymbol{\mu}$ , and precision matrix  $\mathbf{\Omega}$ , whose entries correspond to the partial correlation between the associated variables. In this setting, any two coordinates  $x_a$  and  $x_b$  are conditionally independent given  $x_{-\{a,b\}}$  if and only if the (a,b) entry of the precision matrix  $\mathbf{\Omega}$  is zero (Lauritzen, 1996), and the graph structure can be inferred based on nonzero entries of  $\mathbf{\Sigma}^{-1} := \mathbf{\Omega}$ , also known as the inverse covariance matrix. Throughout the manuscript, we use the terms inverse covariance matrix and precision matrix interchangeably. In practice, the covariance matrix is not known and the graph structure needs to be estimated using samples drawn from an underlying distribution. For example, in a low dimensional setting we can first obtain an estimator of the precision matrix by maximizing the log-likelihood

$$\widehat{\mathbf{\Omega}} = \operatorname{argmax} \quad n \left[ \frac{1}{2} \log \{ \det(\mathbf{\Omega}) \} - \frac{1}{2} \operatorname{tr}(\widehat{\mathbf{\Sigma}} \mathbf{\Omega}) \right], \tag{1}$$

where  $\det(\cdot)$  is the determinant,  $\operatorname{tr}(\cdot)$  is the trace, and  $\widehat{\Sigma} = n^{-1} \sum_{i=1}^{n} (\mathbf{x}_i - \bar{\mathbf{x}}) (\mathbf{x}_i - \bar{\mathbf{x}})^{\top}$  is the empirical covariance matrix. Next, the graph structure is estimated by thresholding small (in absolute value) elements of  $\widehat{\Omega}$  or testing whether they are zero (Drton and Maathuis, 2017), that is, the graph structure corresponds to nonzero entries of the resulting thresholded precision matrix.

In a high-dimensional setting, where the number of parameters to estimate, p, is much larger than the number of data points observed, n, maximizing the log-likelihood (1) results in poor quality estimates. In the particular case of Gaussian data, the resulting estimate, that is, the inverse of the covariance matrix, does not exist when n < p. Unfortunately, the high-dimensional setting is prevalent in various applications. For example, functional imaging of brain measurements using (standard)  $2mm^3$  voxels will result in approximately  $p = O(10^6)$  voxels with  $n = O(10^2)$  measurements (Poldrack et al., 2011; Hsieh et al., 2013). While p is large as compared to n, most entries in  $\Omega$ , denoted as  $\omega_{i,j}$ ,  $i, j = 1, \ldots, p$ , are zero, that is, the inverse covariance matrix is sparse. Hence, a typical strategy to estimate  $\Omega$  in a high-dimensional setting is to add a regularization function, such as the  $\ell_1$ -norm of the parameters, to the log-likelihood function (1), which encourages the graph to be sparse or have other desirable structural biases (Yuan and Lin, 2007; Bühlmann and Van De Geer, 2011). Specifically, we estimate  $\Omega$  using the following optimization program

$$\widehat{\mathbf{\Omega}} = \operatorname{argmax} \quad n \left[ \frac{1}{2} \log \{ \det(\mathbf{\Omega}) \} - \frac{1}{2} \operatorname{tr}(\widehat{\mathbf{\Sigma}} \mathbf{\Omega}) \right] + \lambda_n \sum_{i \neq j} |\omega_{i,j}|.$$
 (2)

Note that regularization is not added to the diagonal terms,  $\omega_{i,i}$ , i = 1, ..., p, because  $\Omega$  is positive definite and adding penalty on the diagonal entries would introduce additional bias. In this manuscript, we focus on simultaneous estimation of multiple graphs that are structurally similar. We will illustrate in the following sections that exploiting the common structures will improve the estimation results on every individual graph.

#### 2.1 Joint Gaussian Graphical Models

We continue to use the example of brain measurements to demonstrate the idea of joint graphical model estimation. Consider the case of n fMRI scans collected from each of the K subjects. Suppose we seek to estimate the functional connectivity (in this case, a graphical model) between the p voxels of each subject k, where p is much greater than n ( $p \gg n$ ). Each functional connectivity network shares similarities with other

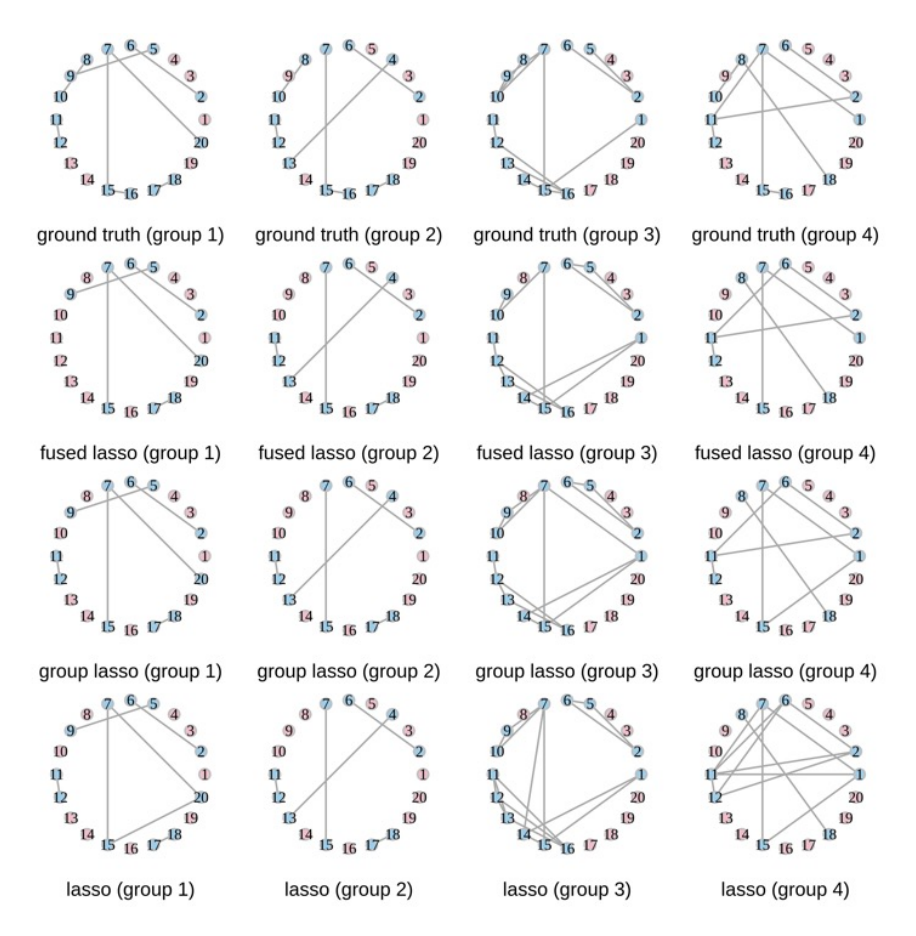


Figure 1: Comparison of joint and separate graph estimation procedures with p = 20 variables and sample size of n = 5000. Pink nodes do not have edges connecting to them, while blue nodes have at least on edge connecting to them. (**Top row**): Ground truth graphs. (**Second row**): Jointly estimated graphs using fused lasso. (**Third row**): Jointly estimated graphs using the group graphical lasso. (**Fourth row**): Graphs estimated separately using the graphical lasso. Details of all methods are provided in the text. From the figure, it is clear that joint estimation significantly outperforms separate estimation.

networks, but are not identical. To better estimate the network of the subject k from n MRI scans, we may borrow information from other networks given that they are expected to share similar patterns. One simple approach is to construct a regularization function that encourages similarities between graphs, an approach known as joint estimation. Figure 1 shows a promising result when one pools the data across subjects, the resulting estimates better recover the ground truth graphs compared to separate estimations. It has also been shown that joint estimation can increase sensitivity and detect edges that are missing in separate estimation (Peterson et al., 2015). Thus, ignoring the information of other groups may lead to suboptimal solutions (Danaher et al., 2014; Lee and Liu, 2015). Moreover, joint estimation of graphical models has been applied successfully in a number of problems, including metabolite experiments (Tan et al., 2017), cancer networks (Mohan et al., 2012; Peterson et al., 2015; Lee and Liu, 2015; Saegusa and Shojaie, 2016; Hao et al., 2018), biomedical data (Yajima et al., 2014; Kling et al., 2015; Pierson et al., 2015), gene expression (Chun et al., 2015; Lin et al., 2017), text processing (Guo et al., 2011), climate data (Ma and Michailidis, 2016), and fMRI (Qiu et al., 2016; Colclough et al., 2018; Skripnikov and Michailidis, 2019; Lukemire et al., 2020). In all of these problems, data are heterogeneous, but the graphs share similarities.

To rigorously describe the example discussed above, we consider the problem of estimating graph structures  $G^{(k)} = (V, E^{(k)})$ , k = 1, ..., K, from K related groups of data. The data for each group are p-variate and share the same set of nodes V, but the underlying connection patterns  $E^{(k)}$  may be different due to

the heterogeneity between groups. The data for the k-th group can be represented as an  $n_k \times p$  matrix  $\mathbf{X}^{(k)} = (\mathbf{x}_1^{(k)}, \dots, \mathbf{x}_{n_k}^{(k)})^{\top}$ , where the rows  $\mathbf{x}_i^{(k)} = (x_{i,1}^{(k)}, \dots, x_{i,p}^{(k)})$ ,  $i = 1, \dots, n_k$ , are p-dimensional vectors of observations. Assuming that the data in each group are distributed according to a p-variate Gaussian distribution,  $\mathbf{x}_i^{(k)} \sim \mathcal{N}(\boldsymbol{\mu}^{(k)}, (\boldsymbol{\Omega}^{(k)})^{-1})$ ,  $i = 1, \dots, n_k$ , where  $\boldsymbol{\mu}^{(k)} \in \mathbb{R}^p$  is the mean, which we assume without loss of generality to be 0, and  $\boldsymbol{\Omega}^{(k)} \in \mathbb{R}^{p \times p}$  is the precision matrix. Given observations  $\mathbf{X} = \{\mathbf{X}^{(1)}, \dots, \mathbf{X}^{(K)}\}$ , we can estimate  $\boldsymbol{\Omega} = \{\boldsymbol{\Omega}^{(1)}, \dots, \boldsymbol{\Omega}^{(K)}\}$  by maximizing the penalized joint log-likelihood for K groups:

$$\widehat{\mathbf{\Omega}} = \operatorname{argmax} \ \widetilde{\ell}(\mathbf{\Omega}) + \mathbf{P}(\mathbf{\Omega}), \qquad \widetilde{\ell}(\mathbf{\Omega}) := \sum_{k=1}^{K} n_k \left[ \log\{\det(\mathbf{\Omega}^{(k)})\} - \operatorname{tr}(\widehat{\mathbf{\Sigma}}^{(k)}\mathbf{\Omega}^{(k)}) \right], \tag{3}$$

where  $\widehat{\mathbf{\Sigma}}^{(k)} = n_k^{-1}(\mathbf{X}^{(k)})^{\top}\mathbf{X}^{(k)}$ ,  $k = 1, \dots, K$ , are the sample covariance matrices. Directly solving (3) without the penalty  $\mathbf{P}(\mathbf{\Omega})$  gives the maximum log-likelihood estimate of  $\mathbf{\Omega}$ . However, the solution is equivalent to solving the maximum log-likelihood estimate of each group individually and fails to utilize the shared "information" across different groups. We hence explore different approaches that use the penalty function  $\mathbf{P}(\mathbf{\Omega})$  to incorporate the group structure and focus on the structural assumptions behind the penalties. The comparison of different methods introduced in the text can be found in Table 1.

The rest of the manuscript is organized as follows. In Section 3, we introduce methods that employ coarse-grained structural constraints, i.e., that each group is equally related to each other. Methods that employ fine-grained structural constraints, i.e., that some groups are more or less correlated with other groups, are discussed in Section 4. Section 5 and 6 illustrate two practical examples. Section 5 covers differential graphs, which are special cases of the joint estimation paradigm with two groups. Joint estimation of time-series data is discussed in Section 6. Finally, in Section 7, we present an empirical evaluation of a variety of regularization methods to evaluate their performance under two graph generation processes: shared inverse covariance structure and shared inverse covariance values. The simulation code is available at https://github.com/koyejo-lab/JointGraphicalLasso.

Table 1: Variants of the joint Gaussian graphical model

Category	Method	Model Name	Model structure $\Omega$	Penalty function/constraint
		JGL (Guo et al., 2011)	$\int \omega_{i,j}^{(k)} = \theta_{i,j} \gamma_{i,j}^{(k)}, \ i \neq j;$	$\lambda_1 \sum_{i \neq j} \theta_{i,j} - \lambda_2 \sum_{k=1}^K \sum_{i \neq j}  \gamma_{i,j}^{(k)} $
			$\omega_{i,i}^{(k)} = \gamma_{i,i}^{(k)}, \ i = j.$	
		JWLGL (Shan et al., 2020)	$\omega_{i,j}^{(k)} = \theta_{m,m'}^{(k)} \gamma_{i,j}^{m,m',(k)}.$	$\lambda_1 \sum_{m \neq m'} \alpha_{m,m'}$
	Penalized		If $m \neq m'$ : $\theta_{m,m'}^{(k)} = \alpha_{m,m'} \beta_{m,m'}^{(k)}$ ,	$+\lambda_2 \sum_{m \neq m'} \sum_{k=1}^K \sum_{i \neq j}  \beta_{m,m'}^{(k)} \gamma_{i,j}^{m,m',(k)} $
	MLE		else if $m = m'$ : $\theta_{m,m}^{(k)} = 1$ and	$+\lambda_3 \sum_{m=1}^{M} \sum_{i \neq j} \iota_{i,j}^{m,m}$
			$\gamma_{i,j}^{m,m,(k)} = \begin{cases} \iota_{i,j}^{m,m} \rho_{i,j}^{m,m,(k)}, & i \neq j; \\ 1 & i = i \end{cases}$	$+\lambda_4 \sum_{m=1}^{M} \sum_{i \neq j} \sum_{k=1}^{K}  \rho_{i,j}^{m,m,(k)} $
Coarse			t = J	
-grained		FGL (Danaher et al., 2014)	$\omega_{i,j}^{(k)}$	$\lambda_1 \sum_{k=1}^{K} \sum_{i \neq j}  \omega_{i,j}^{(k)}  + \lambda_2 \sum_{k < k'} \sum_{i,j}  \omega_{i,j}^{(k)} - \omega_{i,j}^{(k')} $
-gramed		GGL (Danaher et al., 2014)	$\omega_{i,j}^{(k)}$	$\lambda_1 \sum_{k=1}^K \sum_{i \neq j}  \omega_{i,j}^{(k)}  + \lambda_2 \sum_{i \neq j} (\sum_{k=1}^K \omega_{i,j}^{(k)^2})^{\frac{1}{2}}$
		GFGL (Gibberd and Nelson, 2017)	$\omega_{i,j}^{(k)}$	$\lambda_1 \sum_{t=1}^{T} \sum_{i \neq j}  \omega_{i,j}^{(t)}  + \lambda_2 \sum_{t=2}^{T} \ \Omega_{-ii}^{(t)} - \Omega_{-ii}^{(t-1)}\ _F$
		JAGL (Shan and Kim, 2018)	$\left egin{array}{c} \omega_{i,j}^{(k)} \end{array} ight $	$\sum_{k=1}^{K} \frac{1}{n_k} \sum_{i \neq j} \frac{1}{ (1-\pi)\hat{t}_{i,j} + \pi \hat{s}_{i,j}^{(k)} ^r}  \omega_{i,j}^{(k)} ^1$
		TFRE (Bilgrau et al., 2020)	$\omega_{i,j}^{(k)}$	$\sum_{k=1}^K \frac{\lambda_k}{2} \  \mathbf{\Omega}^{(k)} - \mathbf{T}^{(k)} \ _F^2$
				$+\sum_{k_1,k_2}^{K} \frac{\lambda_{k_1,k_2}}{4} \ (\mathbf{\Omega}^{(k_1)} - \mathbf{T}^{(k_1)}) - (\mathbf{\Omega}^{(k_2)} - \mathbf{T}^{(k_2)})\ _F^2$
		RCON (Mohan et al., 2012, 2014)	$\omega_{i,j}^{(k)}$	$G_q(\mathbf{\Omega}^{(1)} - \mathbf{\Omega}^{(2)}) = \min_{V:\mathbf{\Omega}^{(1)} - \mathbf{\Omega}^{(2)} = V + V^{\top}} f(V)$
				$f(V) = \sum_{j=1}^{p} \ V_j\ _q$
	CLIME	JEMP (Lee and Liu, 2015)	$\omega_{i,j}^{(k)} = \theta_{i,j} + \gamma_{i,j}^{(k)}$	$ \frac{1}{K}\sum_{k=1}^{K}\{\widehat{\mathbf{\Sigma}}^{(k)}(\mathbf{\Theta}+\mathbf{\Gamma}^{(k)})-I\} _{\infty}\leq\lambda_{1}$
				$ \widehat{\mathbf{\Sigma}}^{(k)}(\mathbf{\Theta} + \mathbf{\Gamma}^{(k)}) - \mathbf{I} _{\infty} \le \lambda_2, \ \sum_{k=1}^{K} \mathbf{\Gamma}^{(k)} = 0$
	(Cai et al., 2011)	KSE (Qiu et al., 2016)	$\omega_{i,j}^{(k)}$	$ \widehat{\boldsymbol{S}}(u_0)\boldsymbol{\Omega}(u_0) - \boldsymbol{I} _{\infty} \le \xi$
		LASICH (Saegusa and Shojaie, 2016)	$\omega_{i,j}^{(k)}$	$\lambda_1 \sum_{k=1}^K \sum_{i \neq j}  \omega_{i,j}^{(k)} $
Fine	Penalized			$-\lambda_1 \lambda_2 \sum_{i \neq j} (\sum_{k,k'}^K W_{k,k'} (\omega_{i,j}^{(k)} + \omega_{i,j}^{(k')})^2)^{\frac{1}{2}}$
-grained	MLE	GEN-ISTA (Price et al., 2021)	$\omega_{i,j}^{(k)}$	$\lambda_1 \sum_{k=1}^K \sum_{i \neq j}  \omega_{i,j}^{(k)} $
				$+\lambda_2 \sum_{q=1}^{Q} \frac{1}{ D_q } \sum_{k,k' \in D_q} \ \mathbf{\Omega}^{(k)} - \mathbf{\Omega}^{(k)'}\ _F^2$
	Neighborhood	JSEM (Ma and Michailidis, 2016)	$\theta_{i,j}^{(k)} = -\omega_{i,j}^{(k)}/\omega_{i,i}^{(k)}$	$\sum_{j  eq i} \sum_{g \in \mathcal{G}_{i,j}} \lambda_{i,j}^{[g]} \ oldsymbol{ heta}_{i,j}^{[g]}\ _2$
	selection	JMMLE (Majumdar and Michailidis, 2018)		

 $<sup>1 \</sup>over n_k$  denotes the number of samples of group k,  $\hat{t}_{i,j}$  is the precision matrix estimated by pooling all samples across groups,  $\hat{s}_{i,j}$  is the precision matrix estimated by an individual group, and r > 0

# 3 Joint Graphical Models using Coarse-grained Structure

We outline a variety of approaches for joint graphical model estimation that use prior knowledge of coarse-grained structure across groups. The coarse-grained structure, as opposed to fine-grained structure, assumes that the edge structure of each graph has the same degree of similarity among other graphs. In contrast, fine-grained structure assumes local similarity that is only shared within a subset of groups. The performance of the coarse-grained estimation procedure is improved using regularization that captures the common structure across the K groups – enabling the use of shared information across groups. We will discuss two directions in detail: hierarchical regularizers and analogous Bayesian priors.

### 3.1 Joint Graphical Models with Hierarchical Structure

Guo et al. (2011) studied joint estimation of related precision matrices, where the precision matrices are assumed to be related through a hierarchical structure. Specifically, each entry in the precision matrix is the multiplication of a common component across K groups and an individual component:  $\omega_{i,j}^{(k)} = \theta_{i,j} \gamma_{i,j}^{(k)}$  for  $i \neq j$  and  $\omega_{i,i}^{(k)} = \gamma_{i,i}^{(k)}$ , where  $\theta_{i,j}$  is the shared structure and  $\gamma_{i,j}^{(k)}$  is the group-specific component. Thus, this approach enforces a common background structure. To encourage sparsity, an  $\ell_1$ -norm penalty term is also included as a regularizer, resulting in the following objective termed Joint Graphical Lasso (JGL):

$$\widehat{\boldsymbol{\Theta}}, \{\widehat{\boldsymbol{\Gamma}}^{(k)}\}_{k=1}^K = \operatorname{argmax} \ \widetilde{\ell}(\boldsymbol{\Omega}) - \lambda_1 \sum_{i \neq j} \theta_{i,j} - \lambda_2 \sum_{k=1}^K \sum_{i \neq j} |\gamma_{i,j}^{(k)}|,$$

where  $\lambda_1, \lambda_2$  are hyperparameters that control the scale of the penalty. Note that even when the common component  $\theta_{i,j}$  is nonzero, an individual entry  $\omega_{i,j}^{(k)}$  can still be set to zero by the  $\ell_1$  penalty, which denotes a missing edge in the associated graph.

Shan et al. (2020) proposed a joint two-level graphical lasso (JWLGL), which is a more expressive model that constructs two-level structures on both the set of common components and individual components. It further clusters the set of nodes V into M classes and imposes class specific structure: let m and m' be the classes to which nodes i and j belong, respectively. If  $m \neq m'$ , we have:

$$\omega_{i,j}^{(k)} = \theta_{m,m'}^{(k)} \gamma_{i,j}^{m,m',(k)}; \qquad \theta_{m,m'}^{(k)} = \alpha_{m,m'} \beta_{m,m'}^{(k)}.$$

If m = m', we have  $\theta_{m,m}^{(k)} = 1$  and

$$\omega_{i,j}^{(k)} = \theta_{m,m}^{(k)} \gamma_{i,j}^{m,m,(k)}; \qquad \gamma_{i,j}^{m,m,(k)} = \begin{cases} \iota_{i,j}^{m,m} \rho_{i,j}^{m,m,(k)}, & i \neq j; \\ 1, & i = j. \end{cases}$$

Without loss of generality, we assume  $\alpha_{m,m'} \geq 0$  and  $\iota_{i,j}^{m,m} \geq 0$  for  $i \neq j$  and  $m \neq m'$ . Here,  $\alpha_{m,m'}$  and  $\iota_{i,j}^{m,m}$  denote the common components shared across K groups, while  $\beta_{m,m'}^{(k)}$  and  $\rho_{i,j}^{m,m,(k)}$  denote the individual components that vary across groups.

Lee and Liu (2015) proposed a joint estimator of multiple precision matrices (JEMP) under an assumption that precision matrices decompose into the sum of two components:  $\omega_{i,j}^{(k)} = \theta_{i,j} + \gamma_{i,j}^{(k)}$ . In contrast to the maximum likelihood, the estimation procedure of JEMP is motivated by the CLIME estimator (Cai et al., 2011), which estimates a single precision matrix by solving the following optimization problem:

$$\widehat{\mathbf{\Omega}}^{(k)} = \operatorname{argmin} \|\mathbf{\Omega}^{(k)}\|_{1} \quad \text{subject to} \quad |\widehat{\mathbf{\Sigma}}^{(k)}\mathbf{\Omega}^{(k)} - \mathbf{I}|_{\infty} \le \xi, \tag{4}$$

where  $\xi$  is a tuning parameter. The CLIME estimator finds a sparse  $\widehat{\Omega}^{(k)}$  while ensuring that  $\widehat{\Sigma}^{(k)}\widehat{\Omega}^{(k)}$  is close to an identity matrix. JEMP can be seen as a generalization of CLIME to a multi-group setting as it solves the following optimization problem:

$$\widehat{\boldsymbol{\Theta}}, \{\widehat{\boldsymbol{\Gamma}}^{(k)}\}_{k=1}^{K} = \operatorname{argmin} \|\boldsymbol{\Theta}\|_{1} + v \sum_{k=1}^{K} \|\boldsymbol{\Gamma}^{(k)}\|_{1},$$
subject to 
$$\left| \frac{1}{K} \sum_{k=1}^{K} \{\widehat{\boldsymbol{\Sigma}}^{(k)}(\boldsymbol{\Theta} + \boldsymbol{\Gamma}^{(k)}) - \boldsymbol{I} \} \right|_{\infty} \leq \lambda_{1}, \ \left| \widehat{\boldsymbol{\Sigma}}^{(k)}(\boldsymbol{\Theta} + \boldsymbol{\Gamma}^{(k)}) - \boldsymbol{I} \right|_{\infty} \leq \lambda_{2}, \ \sum_{k=1}^{K} \boldsymbol{\Gamma}^{(k)} = 0,$$

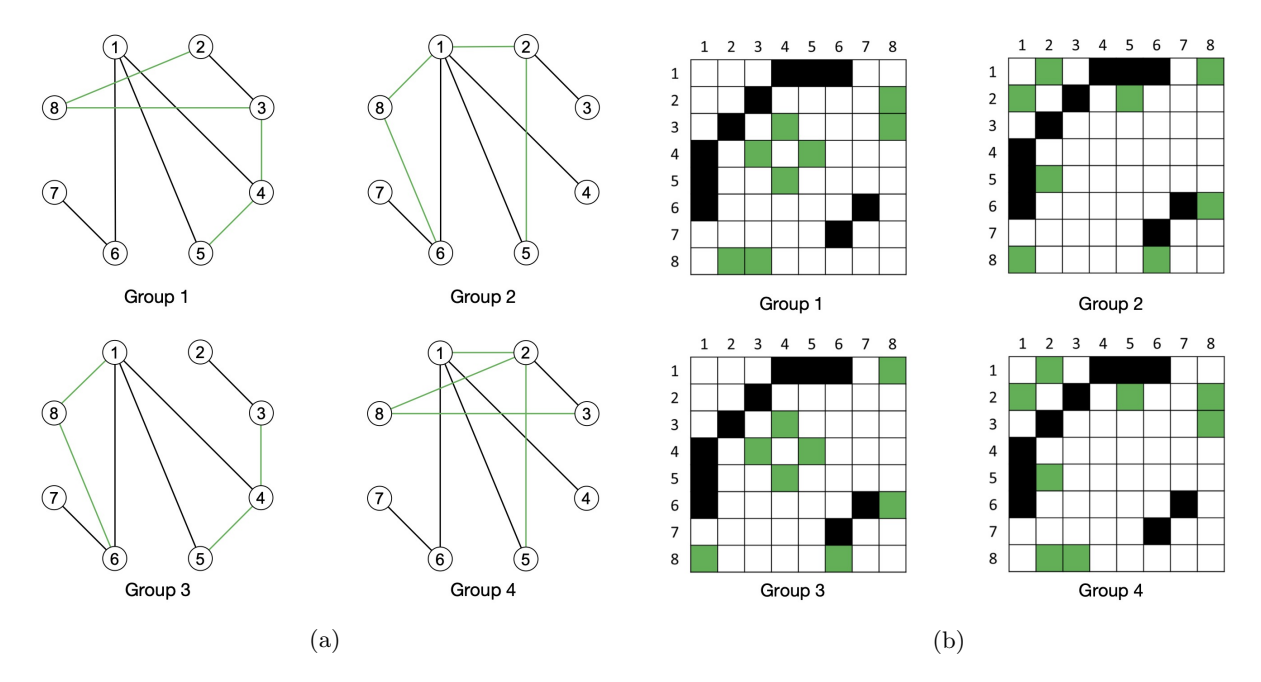


Figure 2: Graphical models with shared coarse-grained structure across groups. (a) The black lines denote the common edges, while green lines denote individual edges. (b) The corresponding adjacency matrices for each graph shown in (a).

where  $\Theta$  denotes the common structure, i.e., the mean of the precision matrices  $K^{-1}\sum_{k=1}^K \Omega^{(k)}$ , and  $\Gamma^{(k)}$  denotes the individual residual components  $\Omega^{(k)} - \Theta$ . In the above optimization problem, the first constraint regularizes the average difference and the second constraint regularizes the individual difference. Thus, the first constraint imposes a common structure across groups. The pre-specified weight v controls the degree of uniqueness of each group, while  $\lambda_1, \lambda_2$  are hyperparameters that measure group average and individual estimation quality, respectively.

#### 3.2 Regularization Approaches for Modeling Joint Structure

Regularization-based approaches (Danaher et al., 2014; Bilgrau et al., 2020; Hao et al., 2018; Shan and Kim, 2018) do not assume the form of the common structure and individual structure, but instead impose similarity constraints across groups. For example, the fused graphical lasso (FGL) and the group graphical lasso (GGL) (Danaher et al., 2014) add convex penalty terms to the log-likelihood function to learn a common structure:

$$\widehat{\mathbf{\Omega}} = \operatorname{argmax} \ \widetilde{\ell}(\mathbf{\Omega}) - \mathbf{P}(\mathbf{\Omega});$$

$$\mathbf{P}_{\text{FGL}}(\mathbf{\Omega}) = \lambda_1 \sum_{k=1}^K \sum_{i \neq j} |\omega_{i,j}^{(k)}| + \lambda_2 \sum_{k < k'} \sum_{i,j} |\omega_{i,j}^{(k)} - \omega_{i,j}^{(k')}|;$$
(5)

$$\mathbf{P}_{GGL}(\mathbf{\Omega}) = \lambda_1 \sum_{k=1}^{K} \sum_{i \neq j} |\omega_{i,j}^{(k)}| + \lambda_2 \sum_{i \neq j} \left( \sum_{k=1}^{K} \omega_{i,j}^{(k)^2} \right)^{\frac{1}{2}}.$$
 (6)

The first penalty term in both  $P_{\text{FGL}}$  and  $P_{\text{GGL}}$  encourages model sparsity. The second term in  $P_{\text{FGL}}$  encourages groups to have shared edge values, while the  $P_{\text{GGL}}$  penalty tends to be less restrictive and only encourages a shared sparsity pattern.

Hao et al. (2018) proposed simultaneous clustering and estimation (SCAN) procedure that addresses the case when the heterogeneous data are missing group labels, e.g., when the groups are latent or unknown.

SCAN partitions the unlabeled data into K clusters and simultaneously imposes a homogeneous structure across groups using the GGL penalty. Given n unlabeled observations  $\boldsymbol{x}_i, i = 1, ..., n$ , with the density function  $l(\boldsymbol{x}, \boldsymbol{\mu}, \boldsymbol{\Omega}) = \sum_{k=1}^K \pi_k l_k(\boldsymbol{x}; \boldsymbol{\mu}^{(k)}, \boldsymbol{\Omega}^{(k)})$ , where  $\pi_k$  is the probability that  $\boldsymbol{x}_i$  belongs to the k-th group and  $l_k(\boldsymbol{x}; \boldsymbol{\mu}^{(k)}, \boldsymbol{\Omega}^{(k)}) = \log\{\det(\boldsymbol{\Omega}^{(k)})\} - \operatorname{tr}\{(\boldsymbol{x} - \boldsymbol{\mu}^{(k)})(\boldsymbol{x} - \boldsymbol{\mu}^{(k)})^{\top}\boldsymbol{\Omega}^{(k)}\}$ . SCAN solves the following optimization problem:

$$\begin{aligned} \{\widehat{\pi}_k\}_{k=1}^K, \widehat{\boldsymbol{\mu}}, \widehat{\boldsymbol{\Omega}} &= \operatorname{argmax} \frac{1}{n} \sum_{i=1}^n \log \left( l(\boldsymbol{x}_i, \boldsymbol{\mu}, \boldsymbol{\Omega}) \right) - \boldsymbol{P}_{SCAN}(\boldsymbol{\mu}, \boldsymbol{\Omega}); \\ \boldsymbol{P}_{SCAN}(\boldsymbol{\mu}, \boldsymbol{\Omega}) &= \lambda_1 \sum_{k=1}^K \sum_{i \neq i} |\omega_{i,j}^{(k)}| + \lambda_2 \sum_{i \neq i} \left( \sum_{k=1}^K \omega_{i,j}^{(k)^2} \right)^{\frac{1}{2}} + \lambda_3 \sum_{k=1}^{n} \sum_{i=1}^p |\mu_i^{(k)}|. \end{aligned}$$

Note that the first two terms of  $P_{SCAN}(\mu, \Omega)$  correspond to the GGL penalty function and the third term is the  $\ell_1$ -norm penalty, used to encourage sparsity.

There are several other methods that use the regularization approach to estimate the joint structure. Shan and Kim (2018) proposed the joint adaptive graphical lasso (JAGL) procedure that introduces a weighted  $\ell_1$  penalty term to tackle problems with unbalanced data. Bilgrau et al. (2020) proposed the targeted fused ridge estimator (TFRE) that uses an additional  $\ell_2$  penalty term that incorporates target matrices as prior information to stabilize the estimation process. Finally, the joint greedy equivalence search (JointGES) procedure uses an  $\ell_0$  penalty term to jointly estimate directed acylic graphs (Wang et al., 2020b).

#### 3.3 Bayesian Methods for Joint Gaussian Graphical Model Estimation

We briefly overview Bayesian methods for joint Gaussian graphical model estimation. Bayesian formulations of graphical models use priors to encourage desired properties for model selection. For example, the Spike-and-slab prior is commonly used in practice to encourage sparsity in precision matrices. In general, the probabilistic counterpart to the penalty function follows the relation  $p(\Omega) \propto \exp(-P(\Omega))$ , where  $p(\Omega)$ is the prior distribution of the precision matrix and  $P(\Omega)$  denotes the penalty function. By Bayes' rule, the posterior distribution is proportional to the product of the likelihood distribution and prior distribution. Therefore, finding the maximum a posteriori (MAP) estimate is equivalent to obtaining the estimate by maximizing the log-likelihood (MLE) with an additional penalty function. Several works (Tan et al., 2017; Li et al., 2019; Yajima et al., 2014; Mitra et al., 2016; Peterson et al., 2015; Lin et al., 2017) have addressed Bayesian graphical model estimation by designing priors that incorporate structural information. In the Gaussian graphical model case, a Wishart prior (Roverato, 2002; Atay-Kayis and Massam, 2005; Lenkoski and Dobra, 2011; Mohammadi et al., 2015) is often placed on the precision matrix. This prior is desirable due to conjugacy, i.e., for a Gaussian likelihood, the posterior distribution remains Wishart. Furthermore, the normalizing constant of the posterior distribution has an explicit form when the graph G is decomposable, that is, when the index set V of a graph can be partitioned into three disjoint nonempty sets  $V = A \cup S \cup B$ and (i) S is a clique, (ii) S separates A and B, (iii)  $A \cup S$  and  $S \cup B$  form decomposable subgraphs.

Li et al. (2019) proposed the joint spike-and-slab graphical lasso prior, designed to encourage global sparse structure. In related work, Tan et al. (2017) placed a multiplicative prior on the adjacency matrices, where the distribution of each edge depends on the multiplication of the values of two end nodes. This prior not only encourages sparsity, but also allows users to specify the degree of connections. We discuss local common structure methods (Peterson et al., 2015; Lin et al., 2017) in Section 4.3 and the differential graph methods (Yajima et al., 2014; Mitra et al., 2016) in Section 5.2. We will not go into details about the Bayesian formulation of graphical models, but instead give a high-level overview of various approaches.

Consider a single group setting with  $\Omega = {\Omega^{(1)}}$ . From a Bayesian perspective, the Lasso regularizer can be viewed as a Laplace prior (Marlin and Murphy, 2009; Wang, 2012) and is formulated as:

$$p(\mathbf{\Omega}|\lambda) = C^{-1} \prod_{i \neq j} \frac{\lambda}{2} \exp\left(-\lambda |\omega_{i,j}|\right) \prod_{i=1}^{p} \left\{ \frac{\lambda}{2} \exp\left(-\frac{\lambda}{2} \omega_{i,i}\right) \mathbb{1}_{(\omega_{i,i} > 0)} \right\} \mathbb{1}(\mathbf{\Omega} \succ 0),$$

where C is the normalizing constant and  $\mathbb{1}(\Omega \succ 0)$  restricts the precision matrix to be positive definite. The term  $\mathbb{1}_{(\omega_{i,i}>0)}$  ensures that the diagonal entries are non-negative and hence preserves the positive definiteness of  $\Omega$ . When taking the logarithm  $\log p(\Omega|\lambda)$ , the first product is equal to the lasso regularizer. Therefore, when computing the MAP estimate, the logarithm of the Laplace prior along with the log-likelihood is the penalized MLE estimator with Lasso penalty function. In the multiple group case, to promote the group similarity between the precision matrices, Li et al. (2019) converted the GGL and FGL penalties to structural priors.

In Bayesian inference, other than computing the MAP estimator, we are also interested in the posterior mean, mode, and samples. In this case, the shrinkage priors are not enough to produce sparse posterior sample (or mean and mode) because the posterior does not concentrate on sparse parameters. Therefore, additional thresholding is required to obtain sparsity. As an alternative, one may use the spike-and-slab prior (Mitchell and Beauchamp, 1988) to promote the sparsity pattern in the posterior. Consider a single group  $\Omega = {\{\Omega^{(1)}\}}$ , the spike-and-slab prior is a hierarchical mixture prior formulated as:

$$p(\mathbf{z}|\lambda) = \prod_{i \neq j} \text{Ber}(z_{i,j}|\lambda);$$
$$p(\mathbf{\Omega}|\mathbf{z}) = \prod_{i \neq j} (1 - z_{i,j}) \delta(\omega_{i,j}) + z_{i,j} \mathcal{N}(\omega_{i,j}|0, \sigma^2),$$

where  $\delta(\cdot)$  denotes the delta function. If  $z_{i,j}=0$ , we restrict the variable to be zero. One may also replace the delta function with a normal distribution with small variance, which approximates the delta function. In the multiple group case, a set of latent indicators following the spike-and-slab distribution adaptively control the value of the FGL (resp., GGL) penalty (Li et al., 2019), namely the Doubly Spike-and-Slab Joint Graphical Lasso (DSS-JGL). Consider two constants  $v_1 > v_0 > 0$  and  $z_{i,j}$ ,  $w_{i,j}$  are binary variables for  $i \neq j$ . We assume that each  $z_{i,j}$  and  $w_{i,j}$  are drawn independently from a Bernoulli distribution with a specific parameter. The DSS-JGL prior is represented as:

$$p(\mathbf{\Omega}|\mathbf{z}, \mathbf{w}) = \lambda_0 \sum_{k=1}^{K} \sum_{i=1}^{p} |\omega_{i,i}^{(k)}| + \lambda_1 \sum_{k=1}^{K} \sum_{i \neq j} \frac{|\omega_{i,j}^{(k)}|}{v_{z_{i,j}}} + \lambda_2 \sum_{i \neq j} \frac{P_*(\mathbf{\Omega})}{v_{(w_{i,j}z_{i,j})}},$$
(7)

where  $P_*(\Omega)$  can be  $P_{\text{FGL}}(\Omega)$  or  $P_{\text{GGL}}(\Omega)$  defined in (5) and (6), respectively. We can choose  $v_0$  to be small, so that when  $z_{i,j} = 0$  for  $i \neq j$ , the second term in (7) will be large, forcing the posterior to be zero. Similar behavior also follows for the joint regularization term in (7) when either  $z_{i,j}$  or  $w_{i,j}$  is zero.

# 4 Joint Graphical Models using Fine-grained Structure

Coarse-grained joint graphical models assume that all groups are equally related; the relation between  $\omega_{i,j}^{(k)}$  and  $\omega_{i,j}^{(k'')}$  and  $\omega_{i,j}^{(k'')}$ ,  $k \neq k', k' \neq k''$  are assumed to be equal. However, in many real world settings, some subsets of groups share local structure that does not appear across all groups. Figure 3 visualizes the adjacency matrices related to edge sets  $E^k$ ,  $k = 1, \ldots, 4$ , of graphical models that are not globally related, but with subsets of the groups that share a local structure. The most common approach in modeling such graphical models is to incorporate this prior knowledge of the relation between subgroups into the estimators (Majumdar and Michailidis, 2018; Ma and Michailidis, 2016; Saegusa and Shojaie, 2016). We briefly outline some approaches for joint graphical model estimation with fine-grained shared structure.

#### 4.1 Entry-wise Structural Information

Given the relation information  $\mathcal{G} = \bigcup_{1 \leq i < j \leq p} \mathcal{G}_{i,j}$ , where  $\mathcal{G}_{i,j}$  is a set that encodes the group relations of node i and node j, Figure 3 (a) illustrates an example of entry-wise structural information. Consider the pair of nodes (i,j) = (3,4) in Figure 3 (a): both graphs of Group 1 and Group 2 have edges (yellow lines) connecting these two nodes, while Group 3 and Group 4 do not have an edge in between. Then the corresponding relation information  $\mathcal{G}_{3,4} = \mathcal{G}_{4,3}$  is  $\{\{1,3\},\{2,4\}\}$ . Similarly, for the pair of

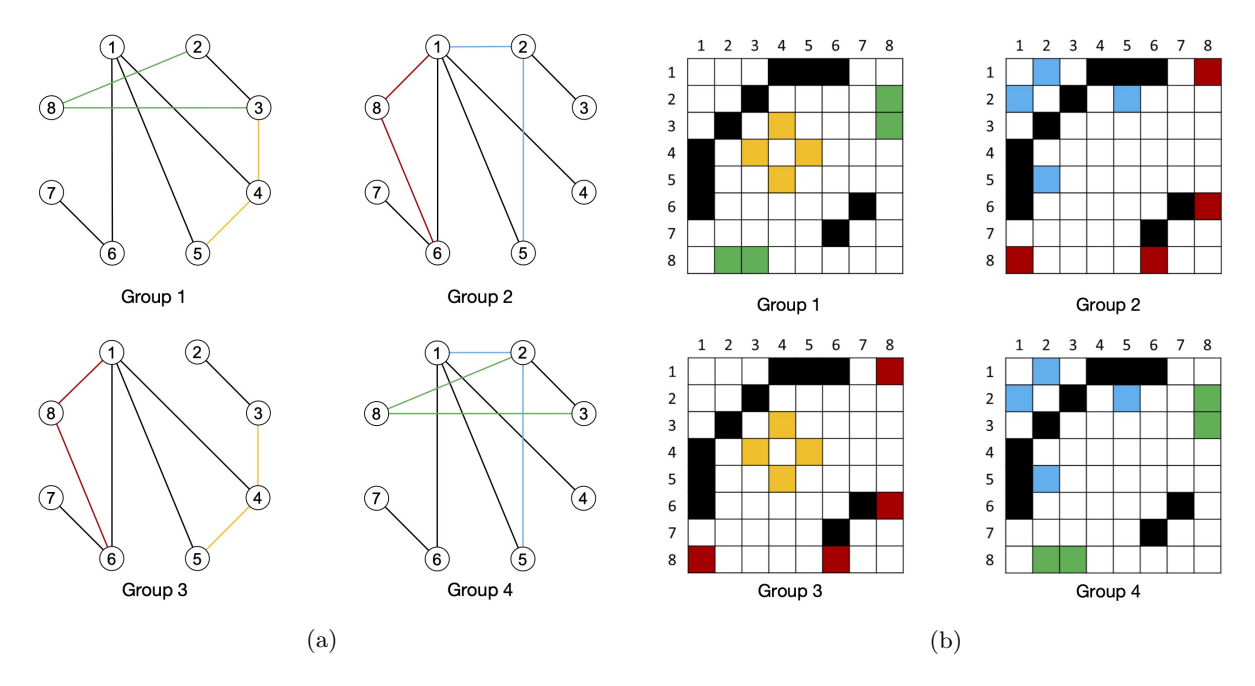


Figure 3: Graphical models with shared fine-grained structure across groups. (a) The black lines denote the common edges. Green colored lines represent the common structure of Group 1 and Group 4, yellow lines of Group 1 and Group 3, red lines of Group 2 and Group 3, and blue lines of Group 2 and Group 4. (b) The corresponding adjacency matrices for each graph shown in (a), using the same colors for groups of shared edges.

nodes (i,j) = (2,8), the graphs of Group 1 and Group 4 have an edge (green line) connecting (2,8), while graphs of Group 2 and Group 3 do not have edge between node (2,8). Then, the corresponding relation information  $\mathcal{G}_{2,8} = \mathcal{G}_{8,2}$  is  $\{\{1,4\},\{2,3\}\}$ . The relation information of graphs in Figure 3 is  $\mathcal{G}_{i,j} = \{\{1,3\},\{2,4\}\}$  for  $(i,j) \in \{(3,4),(4,3),(4,5),(5,4),(1,2),(2,1),(2,5),(5,2)\}$ ;  $\mathcal{G}_{i,j} = \{\{1,4\},\{2,3\}\}$  for  $(i,j) \in \{(2,8),(8,2),(3,8),(8,3),(1,8),(8,1),(6,8),(8,6)\}$ ; and  $\mathcal{G}_{i,j} = \{\{1,2,3,4\}\}$  for the rest of the node pairs.

Ma and Michailidis (2016) proposed a joint structural estimation method (JSEM) to estimate edge sets  $\{\hat{E}^{(k)}\}_{k=1}^K$  by modifying the neighborhood selection algorithm (Meinshausen et al., 2006) to incorporate structural information. Once the edge sets are estimated, each precision matrix is estimated by maximizing the group specific likelihood constrained to have zeros indexed by  $\{\hat{E}^{(k)}\}_{k=1}^K$ . We will briefly introduce the neighborhood selection method and then show how JSEM extends it to multiple graphical models.

The neighborhood selection algorithm estimates the conditional independence structure, which is encoded in the pattern of zeros of the precision matrix under a Gaussian model, by solving a collection of regression problems. See Chapter 12 in (Maathuis et al., 2018) and references therein. Suppose the p-dimensional random variable x follows a normal distribution  $\mathcal{N}(\mu,(\Omega)^{-1})$  with an associated graph G = (V, E). In this case, we can express  $x_i$ ,  $i \in V$ , as a linear function of other nodes:

$$x_i = \sum_{j \in V \setminus \{i\}} \theta_{ij} x_j + \varepsilon_j,$$

where  $\varepsilon_j$  is independent of  $x_j$ ,  $j \in V \setminus \{i\}$ , if and only if  $\theta_{ij} = -\omega_{i,j}/\omega_{i,i}$ . Therefore, the optimal prediction of  $x_i$  given the remaining variables can be formulated as the following optimization problem:

$$\{\widehat{\theta}_{i,j}\}_{j\in V\setminus\{i\}} = \operatorname{argmin} \mathbb{E}\left(x_i - \sum_{j\in V\setminus\{i\}} \theta_{i,j} x_j\right)^2.$$
 (8)

Since the distribution of  $\boldsymbol{x}$  is not known, the expectation term in (8) can not be computed. Let  $\boldsymbol{X}$  be a  $n \times p$  matrix that collects n i.i.d. observations of  $\boldsymbol{x}$ . The  $\ell_1$  penalized empirical optimization objective is the given as:

$$\widehat{\boldsymbol{\Theta}}_{i} = \underset{\boldsymbol{\Theta}_{i}: \, \boldsymbol{\theta}_{i}: \, i=0}{\operatorname{argmin}} \frac{1}{n} \|\boldsymbol{X}_{i} - \boldsymbol{X} \boldsymbol{\Theta}_{i}\|_{2}^{2} + \lambda \|\boldsymbol{\Theta}_{i}\|_{1}, \tag{9}$$

where  $\Theta_i$  is a *p*-dimensional vector  $\Theta_i = (\theta_{i,1}, \dots, \theta_{i,p})^{\top}$ ,  $\theta_{i,i} = 0$ , and  $X_i$  is the *i*-th column of X. To estimate multiple models, JSEM extends the neighborhood selection approach in (9) by solving the following optimization problem:

$$\widehat{\boldsymbol{\Theta}} = \underset{\boldsymbol{\Theta}_{i}^{(k)}: \boldsymbol{\theta}_{i,i}^{(k)} = 0, \ k = 1, \dots, K}{\operatorname{argmin}} \sum_{k=1}^{K} \frac{1}{n_{k}} \|\boldsymbol{X}_{i}^{(k)} - \boldsymbol{X}^{(k)} \boldsymbol{\Theta}_{i}^{(k)}\|_{2}^{2} + 2\boldsymbol{P}_{JSEM}(\{\boldsymbol{\Theta}_{i}^{(k)}\}_{k=1}^{K});$$

$$\boldsymbol{P}_{JSEM}(\{\boldsymbol{\Theta}_{i}^{(k)}\}_{k=1}^{K}) = \sum_{j \neq i} \sum_{g \in \mathcal{G}_{i,j}} \lambda_{i,j}^{[g]} \|\boldsymbol{\theta}_{i,j}^{[g]}\|_{2},$$
(10)

where  $\Theta = \{\Theta^{(1)}, \dots, \Theta^{(K)}\}$ , the penalty term incorporates the relation information  $\mathcal{G}$ , and  $\lambda_{i,j}^{[g]}$  is the group-specific tuning parameter. The penalty function  $P_{JSEM}$  resembles the GGL penalty in (6), except that the norm is now placed on a subset of groups provided by the prior information  $\mathcal{G}$ . Minimizing (10) results in the following estimated edge sets

$$\widehat{E}^{(k)} = \{(i, j) : 1 \le i < j \le p, \widehat{\theta}_{i, j}^{(k)} \ne 0 \text{ or } \widehat{\theta}_{j, i}^{(k)} \ne 0\}, \quad k = 1, \dots, K.$$

Given  $\widehat{E}^{(k)}$ , we define  $\mathcal{S}^+_{\widehat{E}^{(k)}} = \{ \mathbf{\Omega} : \mathbf{\Omega} \succ 0, \ \omega_{i,j} = 0, \ \forall (i,j) \notin \widehat{E}^{(k)} \ \text{and} \ i \neq j \}$ . The precision matrix set  $\mathbf{\Omega}$  is finally estimated by maximizing the log-likelihood with constraints that enforce the sparsity pattern:

$$\widehat{\mathbf{\Omega}}^{(k)} = \underset{\mathbf{\Omega}^{(k)} \in \mathcal{S}_{\widehat{\mathbf{n}}(k)}^{+}}{\operatorname{argmax}} \log \{ \det(\mathbf{\Omega}^{(k)}) \} - \operatorname{tr}(\widehat{\mathbf{\Sigma}}^{(k)} \mathbf{\Omega}^{(k)}), \quad k = 1, \dots, K.$$
(11)

Note that we can apply JSEM only when element-wise structural relation information is given. However, when not all element-wise structural relation information is provided, one can still use the GGL penalty on subsets of groups for which prior information is available.

#### 4.2 Group-wise Structural Information

As obtaining entry-wise structural information is sometimes challenging, another approach is to use the relationship between groups, described by weights, in estimation. For example, suppose that K=3 and we have the following relationships between groups: Group 1 and Group 2 share similarity, Group 1 and Group 3 also share similarity, but Group 2 and Group 3 are unlikely to be similar. To this end, Saegusa and Shojaie (2016) proposed LASICH (Laplacian shrinkage for inverse covariance matrices from heterogeneous populations), that uses a weighted graph  $G_g=(\Gamma,E,W)$  to record the group relation. The node set  $\Gamma$  denotes K groups, the edge set E captures the relations between groups, and the weight set  $W:E\to\mathbb{R}_+$  represents the similarities between groups. Then, a Laplacian penalty function is placed on the objective function to impose group similarity. The optimization problem is formulated as follows:

$$\begin{split} \widehat{\boldsymbol{\Omega}} &= \operatorname{argmax} \ \widetilde{\ell}(\boldsymbol{\Omega}) - \boldsymbol{P}_{LASICH}(\boldsymbol{\Omega}), \\ \text{subject to } \boldsymbol{\Omega}^{(k)} &= (\boldsymbol{\Omega}^{(k)})^{\top}, \ \boldsymbol{\Omega}^{(k)} \in \mathcal{S} \succ 0, \quad k = 1, \dots, K; \\ \boldsymbol{P}_{LASICH}(\boldsymbol{\Omega}) &= \lambda_1 \sum_{k=1}^K \sum_{i \neq j} |\omega_{i,j}^{(k)}| - \lambda_1 \lambda_2 \sum_{i \neq j} \left( \sum_{k,k'}^K W_{k,k'} \left( \omega_{i,j}^{(k)} + \omega_{i,j}^{(k')} \right)^2 \right)^{\frac{1}{2}}, \end{split}$$

where the first penalty term in  $P_{LASICH}(\Omega)$  promotes the sparsity pattern and the second term encourages the similarities within subsets of groups. Although the three approaches (Majumdar and Michailidis, 2018;

Ma and Michailidis, 2016; Saegusa and Shojaie, 2016) discussed here require prior information on the group relation, they provide a more flexible structure than the global structure methodologies, such as GGL (Danaher et al., 2014) and (Guo et al., 2011). In particular, the global structure approach can be viewed as a special case of a local structure approach with homogeneous structural information.

While the work introduced earlier required prior information about the group relation, which may not be available for most cases, Graphical Elastic Net Iterative Shrinkage Thresholding Algorithm (GEN-ISTA) (Price et al., 2021) jointly estimates graphs and group members via k-means clustering. Assume that we want to further cluster group k = 1, ..., K into Q classes, and we denote  $D_q$  for q = 1, ..., Q as the set that contains the group membership. Its objective function is as follows

$$\underset{\boldsymbol{\Omega}, \boldsymbol{D}}{\operatorname{argmin}} \widetilde{\ell}(\boldsymbol{\Omega}) - \mathbf{P}_{GEN-ISTA}(\boldsymbol{\Omega}, \boldsymbol{D});$$

$$\mathbf{P}_{GEN-ISTA}(\boldsymbol{\Omega}, \boldsymbol{D}) = \lambda_1 \sum_{k=1}^{K} \sum_{i \neq j} |\omega_{i,j}^{(k)}| + \lambda_2 \sum_{q=1}^{Q} \frac{1}{|D_q|} \sum_{k, k' \in D_q} \|\boldsymbol{\Omega}^{(k)} - \boldsymbol{\Omega}^{(k)'}\|_F^2.$$

$$(12)$$

GEN-ISTA can be implemented via alternating minimization. It is easy to see that when we fix  $\Omega$  and optimize D, then (12) becomes a k-means clustering objective.

#### 4.3 Bayesian Approach

We introduce two Bayesian methods that construct priors to constrain the similarities within subsets of groups. Unlike the structural regularization approaches introduced in Section 4.1, both methods we discuss here do not require specific prior information on each graph but employ a general prior distribution to build the group relations. This property is particularly desirable because, in most cases, we may not have the structural information for K groups of data.

Peterson et al. (2015) proposed the Markov Random Field (MRF) prior for the graphs  $G^{(k)} = (V, E^{(k)}), k = 1, ..., K$  to encourage the selection of edge indices in related graphs. In addition, the selection of edge indices is controlled by two variables: a random matrix  $\Theta$ , which measures the degree of similarity between groups and an edge-specific coefficient vector  $\mathbf{v}$  reflecting the probability of the corresponding edge being selected. Higher value of  $v_{i,j}$  means that the edge connecting the i-th node and j-th node is more likely to be selected. As a result,  $\mathbf{v}$  is capable of controlling the sparsity of graphs. The Beta prior is placed on  $\mathbf{v}$ , in which the distribution features a higher probability for lower values, indicating that edges are not likely to exist in graphs. Meanwhile, the spike-and-slab prior is placed on the group similarity matrix  $\Theta$  to allow discrimination between zero similarity and positive similarity. Finally, the precision matrices are estimated conditional on the graph structures  $G^{(k)} = (V, E^{(k)}), k = 1, ..., K$  using the G-Wishart prior.

# 5 Estimating Differential Graphical Models

In contrast to joint estimation, several applications in biomedical research, such as analyzing the gene expression differences in normal cells and cancer cells or differences between the test group and control group, consider the case where K=2. Different from the methods in Section 3–4, we will be focusing on finding the "differences" rather than finding the "similarities". In the high dimensional setting, we assume that the difference of two graphs is sparse. Although the differences between two graphs can be naively estimated by using a joint estimation method first and then finding the difference, procedures that directly estimate the difference are statistically more efficient (Shojaie, 2021).

In this section, we briefly overview two approaches that estimate graph differences, the direct estimation method and the regularization based approach. For a detailed introduction, see Shojaie (2021) for a recent review.

#### 5.1 Direct Estimation

The direct approach estimates the difference  $\Delta = \Omega^{(1)} - \Omega^{(2)}$  without explicitly estimating individual precision matrices  $\Omega^{(1)}$  and  $\Omega^{(2)}$ . This approach potentially fits a broader class of precision matrices as the individual precision matrices,  $\Omega^{(1)}$  and  $\Omega^{(2)}$ , need not be sparse, but only the difference  $\Delta$  is assumed sparse. In addition, jointly estimating  $\Omega^{(1)}$  and  $\Omega^{(2)}$  can be challenging when the sparse assumption is violated. Zhao et al. (2014) directly estimated the difference  $\Delta$  by solving a constrained minimization problem, noting that, by definition, we have  $\Sigma^{(1)}\Delta\Sigma^{(2)} - \Sigma^{(1)} + \Sigma^{(2)} = \mathbf{0}$ . Consequently, estimating the differential graph  $\Delta = \Omega^{(1)} - \Omega^{(2)}$  can be achieved by minimizing the following objective:

$$\widehat{\boldsymbol{\Delta}} = \operatorname{argmin} \|\boldsymbol{\Delta}\|_1$$
, subject to  $\left|\widehat{\boldsymbol{\Sigma}}^{(1)} \boldsymbol{\Delta} \widehat{\boldsymbol{\Sigma}}^{(2)} - \widehat{\boldsymbol{\Sigma}}^{(1)} + \widehat{\boldsymbol{\Sigma}}^{(2)}\right|_{\infty} \leq \lambda_1$ ,

which is an extension of the CLIME (Cai et al., 2011) method. Xu and Gu (2016); Yuan et al. (2017) utilized the symmetry property  $\Sigma^{(1)} \Delta \Sigma^{(2)} = \Sigma^{(2)} \Delta \Sigma^{(1)}$  and hence  $2^{-1} (\Sigma^{(1)} \Delta \Sigma^{(2)} + \Sigma^{(2)} \Delta \Sigma^{(1)}) - \Sigma^{(1)} + \Sigma^{(2)} = \mathbf{0}$ . They defined the objective function as

$$\begin{split} \widehat{\boldsymbol{\Delta}} &= \operatorname{argmin} \widehat{\ell}(\boldsymbol{\Delta}) + \lambda_1 \|\boldsymbol{\Delta}\|_1; \\ \widehat{\ell}(\boldsymbol{\Delta}) &= \frac{1}{2} \operatorname{tr}(\boldsymbol{\Delta} \widehat{\boldsymbol{\Sigma}}^{(1)} \boldsymbol{\Delta} \widehat{\boldsymbol{\Sigma}}^{(2)}) - \operatorname{tr} \left\{ \boldsymbol{\Delta} (\widehat{\boldsymbol{\Sigma}}^{(1)} - \widehat{\boldsymbol{\Sigma}}^{(2)}) \right\}, \end{split}$$

where the Hessian of the objective with respect to  $\Delta$  is  $(\widehat{\Sigma}^{(1)} \otimes \widehat{\Sigma}^{(2)} + \widehat{\Sigma}^{(2)} \otimes \widehat{\Sigma}^{(1)})/2$ , which is positive semi-definite. Therefore,  $\widehat{\ell}(\Delta) + \lambda_1 \|\Delta\|_1$  is a convex function with respect to  $\Delta$ , hence a unique minimizer exists. Other recent work extends the direct estimation approach to more expressive structured differential graphs. Na et al. (2021) constructed a latent structure estimator where the underlying difference can be formulated as a sum of low-rank matrix and sparse matrix – a framework first discussed by (Chandrasekaran et al., 2012). Zhao et al. (2019) extended the direct estimation approach to estimating the differential graph of functional data.

## 5.2 Regularization based approach

The node-based learning framework (Mohan et al., 2012, 2014) assumes that most parts of the graph are shared, and the difference is generated by a node perturbation. When a node is perturbed, the edges connecting this node to others change across K groups. In addition to maximizing the degree of the overlapping structure between groups, the task is to detect perturbed nodes. An intuitive way to look for the perturbed node is to look at the difference of two graphs  $\Omega^{(1)} - \Omega^{(2)}$ . When the j-th node is being perturbed, the corresponding j-th row and j-th column of  $\Omega^{(1)} - \Omega^{(2)}$  will have non-zeros, constructing a unique symmetric row-column group. Given that there are several nodes being perturbed,  $\Omega^{(1)} - \Omega^{(2)}$  will be the union of the row-column groups, each stemming from a perturbed node. Using this concept, the Row-Column Overlap Norm (RCON) (Mohan et al., 2012, 2014) is designed to encourage sparsity in the union of the row-column groups:

$$\begin{split} \boldsymbol{P}_{\text{RCON}}(\boldsymbol{\Omega}) &= \lambda_1 \sum_{k=1}^2 \sum_{i,j} |\omega_{i,j}^{(k)}| + \lambda_2 G_q(\boldsymbol{\Omega}^{(1)} - \boldsymbol{\Omega}^{(2)}); \\ G_q(\mathbf{A}) &= \min_{\mathbf{V}: \mathbf{A} = \mathbf{V} + \mathbf{V}^\top} f(\mathbf{V}); \\ f(\mathbf{V}) &= \sum_{j=1}^p \|\mathbf{v}_j\|_q, \end{split}$$

where  $\mathbf{v}_j$  is the j-th column of  $\mathbf{V}$ . It is easy to see that when q=1, the RCON penalty is equivalent to the FGL penalty in (5). This penalty function simultaneously imposes sparse structure on both the individuals ,  $\mathbf{\Omega}^{(1)}$  and  $\mathbf{\Omega}^{(2)}$ , and the difference  $\mathbf{\Omega}^{(1)} - \mathbf{\Omega}^{(2)}$ . As mentioned earlier, this method may not work well under the setting that  $\mathbf{\Omega}^{(1)}$  and  $\mathbf{\Omega}^{(2)}$  are not sparse.

To infer the relative differences between two graphs in a Bayesian formulation, it is intuitive to place a prior on the the differences of two graphs  $\theta_{i,j} = E_{i,j}^{(1)} - E_{i,j}^{(1)}$ , for every i < j. Since the difference  $\theta_{i,j}$  is binary, either 0 (no difference) or 1 (difference), an example (Mitra et al., 2016) is to place a Bernoulli distribution  $Ber(\pi)$  on  $\theta_{i,j}$ , i < j where  $\pi$  follows Beta distribution, specifying the tendency of being different on two graphs.

## 6 Graphical Models for Time Series Data

Time-varying graphical models (Zhou et al., 2010a; Kolar et al., 2010; Zhu and Koyejo, 2018) can be seen as extensions of joint graphical models with groups organized along the time index. The samples are assumed to be generated as  $\mathbf{x}_i^{(t)} \sim \mathcal{N}(\boldsymbol{\mu}^{(t)}, (\boldsymbol{\Omega}^{(t)})^{-1}), i = 1, \dots, n_t$ , where  $t = 1, \dots, T$  is the time index. Under such a model, the estimation of time-varying precision matrices and corresponding dynamic networks is challenging as data scarcity is a serious issue: in many problems, we only observe a single sample at each time point. Therefore, to make the estimation possible, structural assumptions are imposed on how the underlying precision matrices and dynamic networks change over time. Such assumptions control the model complexity and allow for the development of estimation procedures. Examples of structural assumptions on temporal dynamics include piece-wise constant and smoothly changing precision matrices, as well as combinations of both. Piece-wise constant structure captures discrete temporal evolution from one stage to another. For example, the gene regulatory network in a fruit-fly can undergo structural changes as the fruit-fly develops from an embryo to an adult state. Smooth temporal structure can be used to model the dynamic functional connectivity of brain networks that exhibit smooth temporal evolution from one brain state to another (Shine et al., 2016). The temporal dynamics of crime rates are often modeled as a combination of smooth dynamics and sudden jumps, where the jumps capture sudden serious crime events. In this section, we will discuss how to apply the FGL penalty and its variants to build piece-wise constant structure. We also introduce a joint estimation framework of multiple autoregressive models to model smooth temporal data.

### 6.1 Regularized Estimation

The FGL penalty has been widely used in time-varying graphical models to model piece-wise constant dynamics (Kolar et al., 2010; Kolar and Xing, 2012; Monti et al., 2014; Hallac et al., 2017). For instance, Smooth Incremental Graphical Lasso Estimation (SINGLE) (Monti et al., 2014) applies the FGL framework to enforce similarity between consecutive precision matrices:

$$\mathbf{P}_{SINGLE}(\mathbf{\Omega}) = \lambda_1 \sum_{t=1}^{T} \sum_{i \neq j} |\omega_{i,j}^{(t)}| + \lambda_2 \sum_{t=2}^{T} \sum_{i \neq j} |\omega_{i,j}^{(t)} - \omega_{i,j}^{(t-1)}|.$$
 (13)

The first term encourages the sparsity of each graph and the second term regularizes the "jumps" across time. On the other hand, Group-Fused Graphical Lasso (GFGL) (Gibberd and Nelson, 2017) introduces the Frobenius norm as an alternative to encourage neighbouring similarity:

$$\mathbf{P}_{GFGL}(\mathbf{\Omega}) = \lambda_1 \sum_{t=1}^{T} \sum_{i \neq j} |\omega_{i,j}^{(t)}| + \lambda_2 \sum_{t=2}^{T} \|\mathbf{\Omega}_{-ii}^{(t)} - \mathbf{\Omega}_{-ii}^{(t-1)}\|_F,$$

where  $\Omega_{-ii}^{(t)}$  denotes the precision matrix  $\Omega^{(t)}$  with the diagonal part removed. One may wonder what the differences in structure assumptions are between the Frobenius norm and the  $\ell_1$ -norm in (13). The  $\ell_1$ -norm regularizes individual changes, while the Frobenius norm assumes global changes, implying that several edges within a graph will change simultaneously.

While methods introduced in the last paragraph encourage similarity of two neighboring graphs, the graph that is one-step ahead and that of one-step behind, another idea is to enforce the similarities within multiple steps ahead and behind. This can be done by creating a moving window index set (Yang and Peng, 2020)  $\mathcal{N}_w(t)$  for each time point t = 1, ..., T. Consider a window of length 2w. At every time point t, we look at data w-steps ahead and w-steps behind and hence the index set is  $\mathcal{N}_w(t) = \{i = 1, ..., T : |t - i| \le 2w\}$ .

Note that the index set  $\mathcal{N}_w(t)$  also includes t itself. Then, we apply the GGL penalty to the components in the index set.

### 6.2 Kernel Smoothing Graphical Models

Another way to construct smoothly varying graphs is by using an autoregressive structure. This model assumes that each data point is a linear combination of previous data points with additional independent noise. Consider the lag-1 case, where  $\mathbf{x}^{(t)}$  is a linear transform of  $\mathbf{x}^{(t-1)}$  with independent noise  $\boldsymbol{\varepsilon}^{(t)} \sim \mathcal{N}(\mathbf{0}, \mathbf{G}^{(t)})$ :

$$\mathbf{x}^{(t)} = \mathbf{A}\mathbf{x}^{(t-1)} + \boldsymbol{\varepsilon}^{(t)}, \quad t = 1, \dots, T,$$

where  $\mathbf{A} \in \mathbb{R}^{p \times p}$  is the transition matrix. Consequently, the covariance matrix is smoothly varying along t if  $\mathbf{G}^{(t)}$  is a smooth function of t:

$$\mathbf{\Sigma}^{(t)} = \mathbf{A}\mathbf{\Sigma}^{(t-1)}\mathbf{A}^T + \mathbf{G}^{(t)}, \quad t = 1, \dots, T.$$
(14)

Motivated by this structure, Zhou et al. (2010b) proposed a kernel based method to estimate a smooth time-varying covariance structure. First, a weighted sum of the sample covariance matrices  $\widehat{\Sigma}^{(1)}, \dots, \widehat{\Sigma}^{(T)}$  is computed as

$$\widehat{\mathbf{S}}^{(t)} = \frac{\sum_{s=1}^{T} w(s,t) \widehat{\mathbf{\Sigma}}^{(s)}}{\sum_{s'=1}^{T} w(s',t)},$$

where the weights are constructed by a symmetric nonnegative kernel function K(|s-t|/h). This ensures that the estimated covariance is smoothly varying over time. Subsequently, the precision matrix is estimated using the following objective:

$$\widehat{\mathbf{\Omega}}^{(t)} = \operatorname{argmax} \quad n \left[ \frac{1}{2} \log \{ \det(\mathbf{\Omega}^{(t)}) \} - \frac{1}{2} \operatorname{tr}(\widehat{\mathbf{S}}^{(t)} \mathbf{\Omega}^{(t)}) \right] + \lambda_n \sum_{i \neq j} |\omega_{i,j}^{(t)}|, \quad t = 1, \dots, T.$$

The kernel smoothing method can also be extended to model two-way continuous changes. For instance, the ages of subjects from the fMRI dataset vary across an interval, and one can parametrize the transition matrices as A(u) with u taking values in a closed subset of the real line. This model is smooth in two aspects: across the temporal domain and labels (groups). Hence, we have the following autoregressive model:

$$\mathbf{x}_{i,t} = \mathbf{A}(u_i)\mathbf{x}_{i,t-1} + \boldsymbol{\varepsilon}_{i,t}, \quad i = 1,\dots,n, \ t = 2,\dots,T.$$
  
$$\mathbf{\Sigma}(u) = \mathbf{A}(u)\mathbf{\Sigma}(u)\mathbf{A}(u)^{\top} + \sigma^2 \mathbf{I}.$$

The Kernel-Smoothing Estimator (KSE) (Qiu et al., 2016) is a kernel based estimator for the covariance matrix and then uses the CLIME (Cai et al., 2011) method introduced in Section 3.1 to recover precision matrices. We consider a set of n data  $Y = \{y_1, \ldots, y_n\}$ , where  $y_i = \{y_{i,1}, \ldots, y_{i,T}\} \in \mathbb{R}^{p \times T}$  and with label  $u_i \in [0, 1]$ . The estimated covariance model of the label  $u_0 \in [0, 1]$  is formulated as the following:

$$\widehat{\boldsymbol{S}}(u_0) = \sum_{i=1}^n w_i(u_0, h) \widehat{\boldsymbol{\Sigma}}_i;$$

$$w_i(u_0, h) := \frac{c(u_0)}{nh} K\left(\frac{u_i - u_0}{h}\right);$$

$$c(u_0) = \begin{cases} 2\boldsymbol{I}, \ u_0 \in \{0, 1\}, \\ 1\boldsymbol{I}, \ u_0 \in (0, 1), \end{cases};$$

$$\widehat{\boldsymbol{\Sigma}}_i = \frac{1}{T} \sum_{t=1}^T \boldsymbol{y}_{i,t} \boldsymbol{y}_{i,t}^\top,$$

where  $w_i$  is the kernel-based weight with predefined scale h,  $K(\cdot)$  is the kernel,  $c(u_0)$  determines the boundary value, and  $\hat{\Sigma}_i$  is the sampled covariance of the time-series data. After obtaining  $\hat{S}(u_0)$ , the precision matrix  $\hat{\Omega}(u_0)$  is obtained using CLIME (Cai et al., 2011) in (4):

$$\widehat{\mathbf{\Omega}}(u_0) = \operatorname{argmin} \|\mathbf{\Omega}(u_0)\|_1,$$
  
subject to  $|\widehat{\mathbf{S}}(u_0)\mathbf{\Omega}(u_0) - \mathbf{I}|_{\infty} \le \xi.$ 

Under this framework, the kernel trick is used to capture the assumption that the covariance matrices are smoothly varying across labels. In addition, the Euclidean distance of two labels reflects the similarity of the two groups, capturing the dependence structure. The kernel-based method can be applied to general joint estimation, where the sampled covariance of time-series data is replaced by the sample covariance of data with the same labels.

## 7 Experiments

We demonstrate that methods that jointly estimate graphs perform better than methods that estimate them separately, both in terms of edge recovery and graph estimation. The quality of edge recovery is evaluated via the Receiver Operating Characteristic (ROC) curve. The quality of graph estimation is evaluated via the entropy loss – which requires the knowledge of the ground truth precision matrix to compute. In the absence of ground truth parameters, we evaluate the quality of the graph estimation by splitting the data into two batches. We use one batch for estimation and the other batch for evaluation by computing the out-of-sample log-likelihood.

To evaluate the performance of joint estimation compared to separate estimation, we examine three regularization methods that capture the key properties of each family of models: the group graphical lasso, which is a canonical example of JSEM (Ma and Michailidis, 2016), LASICH (Saegusa and Shojaie, 2016), JAGL (Shan and Kim, 2018), JMMLE (Majumdar and Michailidis, 2018); the fused graphical lasso, which is a canonical example of GFGL (Gibberd and Nelson, 2017), TFRE (Bilgrau et al., 2020), GEN-ISTA (Price et al., 2021), and the graphical lasso method – which does not incorporate joint information. The first two penalty functions encourage similarities between groups, while the last one only encourages sparsity within groups. We evaluate the performance of these methods under different data generating processes.

#### 7.1 Experiment setup

The graph  $G^{(k)}$  of each group is obtained as the union of a shared component  $G_s = (V, E_s)$  and an individual component  $G_i^{(k)} = (V, E_i^{(k)})$ , that is,  $G^{(k)} = (V, E_s \cup E_i^{(k)})$ . The shared component is a scale-free graph, whose degree follows a power distribution. An individual component is generated as an Erdős Rényi random graph, where  $\rho$  specifies the ratio of edges being connected (in most settings, we set  $\rho = 0.1$ ). We consider two settings. Data Generation Process 1 (DGP1) has a partially shared support of the inverse covariance, with the entries on the shared support also sharing values. Data Generation Process 2 (DGP2) only has a shared support, but the corresponding inverse covariance matrix differs across groups.

#### 7.2 Evaluation of Edge Selection

We summarize the performance of each approach using the Receiver Operating Characteristic (ROC) curve, where the x-axis denotes the false positive rate (FPR) of the estimated edges and the y-axis denotes the true positive rate (TPR) of the estimated edges. The ideal estimator is an estimator that has the true positive rate of 1 and false positive rate of 0, and hence (FPR, TPR)= (0,1) is at the upper left corner of the ROC plot. This implies that the estimator selects all true edges and does not include any false edges of the graph. If the estimator selects all edges of a graph, then both the TPR and FPR are 1. Then, under this scenario, (FPR, TPR)= (1,1) is at the upper right corner of the ROC plot. Similarly, if the model does not select any

edge, then both the FPR and TPR are 0, resulting (FPR, TPR)=(0,0) located on the bottom left of the ROC plot. When we vary  $\lambda_1$ , which determines the strength of the sparsity of individual component  $\omega_{i,j}^{(k)}$  for  $i \neq j$  and  $k = 1, \ldots, K$ , as shown in (5)–(6), it controls the FPR and TPR of the underlying estimator. Plotting (FPR, TPR) under different choices of  $\lambda_1$  results in the ROC curve.

Since (FPR, TPR)=(0,1) is rarely achievable, and the extreme cases (FPR, TPR)=(1,1), (0,0) do not provide useful results, one may restrict the value for either rate and optimize for the other rate. That is, given a fixed TPR tolerance, we would like the FPR to be as small as possible. On the other hand, given a fixed FPR tolerance, we want the TPR rate to be as large as possible. In principle, a good model forms a ROC curve that is curved to the upper left corner, which is toward (FPR, TPR)=(0,1), and hence it has a large Area Under the ROC Curve (AUC). Consequently, we can use the AUC to compare different models.

In our experiments, each ROC curve is computed by tuning the penalty parameter  $\lambda_1$  over the range [0.01, 0.3] and averaging results over 20 independent simulation runs. Recall  $\lambda_2$  controls the sparsity pattern of the shared components, as demonstrated in (5)–(6). We tune the penalty parameter  $\lambda_2$  over 8 different values,  $\lambda_2 \in \{0.025, 0.05, 0.075, 0.1, 0.125, 0.15, 0.175, 0.2\}$ , and pick the value that has the largest AUC. We set p = 100, n = 50, K = 5, and  $\rho = 0.1$ . The false-positive rate is defined as:

$$\frac{1}{K} \sum_{k=1}^{K} \frac{\sum_{i,j} I(\omega_{i,j}^{(k)} = 0, \widehat{\omega}_{i,j}^{(k)} \neq 0)}{\sum_{i,j} I(\omega_{i,j}^{(k)} = 0)},$$

and the false negative rate is defined as:

$$\frac{1}{K} \sum_{k=1}^{K} \frac{\sum_{i,j} I(\omega_{i,j}^{(k)} \neq 0, \widehat{\omega}_{i,j}^{(k)} = 0)}{\sum_{i,j} I(\omega_{i,j}^{(k)} \neq 0)},$$

where  $I(\cdot)$  is the indicator function,  $\omega_{i,j}^{(k)}$  is the i,j-th component of the ground truth inverse covariance matrix of group k,  $\widehat{\omega}_{i,j}^{(k)}$  is the i,j-th component of the estimated inverse covariance matrix of group k. In practice, we use the truncation method to replace the zero-threshold identity function  $I(\cdot)$ . That is, adding a threshold to the identity function:  $I(|\omega_{i,j}^{(k)}| \geq \varepsilon)$ , where  $\varepsilon$  is a predefined threshold to replace  $I(\omega_{i,j}^{(k)} \neq 0)$ , where  $\varepsilon$  is selected to be  $10^{-3}$  in our simulations. The same mechanism works for the case when  $I(\omega_{i,j}^{(k)} = 0)$ . This approach leads to less noisy recovery.

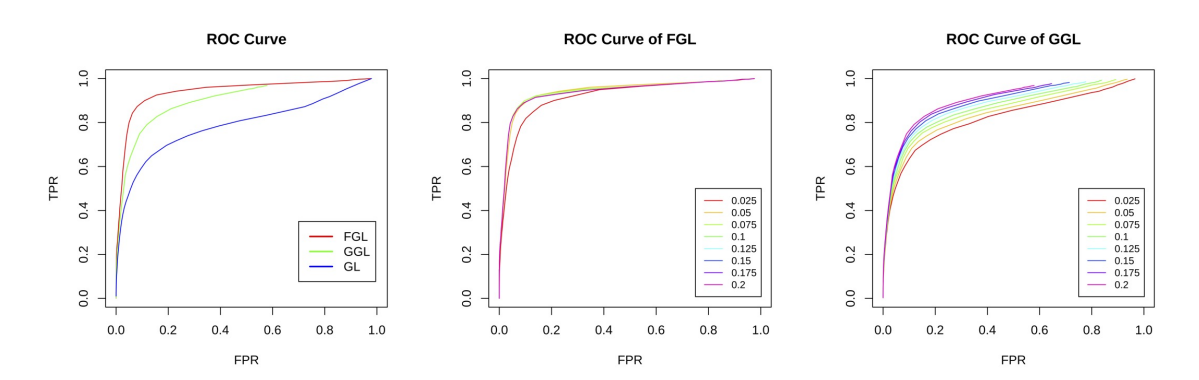


Figure 4: DGP1 features shared structure with the same inverse covariance values. In this case, the fused graphical lasso is expected to achieve the best performance. The experiment results in the **left** figure demonstrates our expectation. The **center** and **right** figures show the ROC curve of fused graphical lasso and group graphical lasso for different  $\lambda_2$  values. While changing the  $\lambda_2$  in the **center** figure does not show obvious differences, the larger  $\lambda_2$  in **right** figure shows better performance.

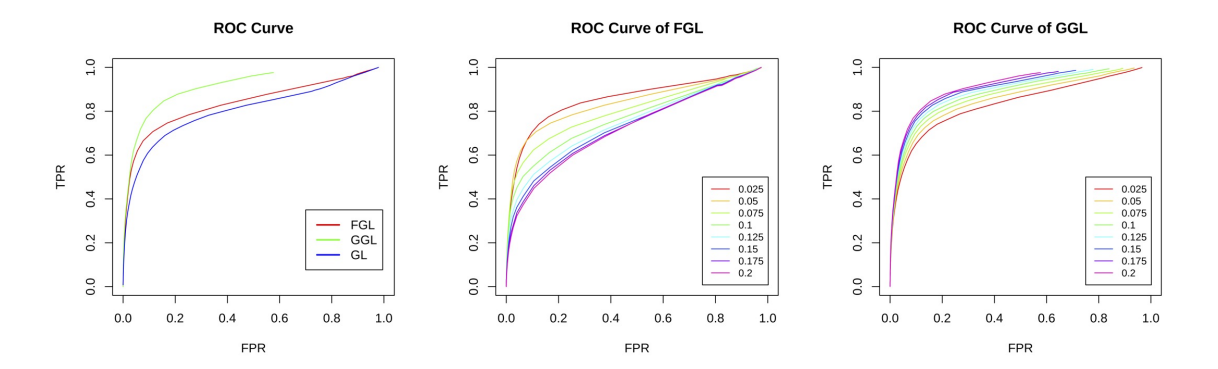


Figure 5: DGP2 features a shared structure with different inverse covariance values. In this case, the group graphical lasso is expected to achieve the best performance. The experiment results in **left** figure reflect our expectations. The **center** figure and **right** figure shows the ROC curve of fused graphical lasso and group graphical lasso under different  $\lambda_2$  values. In the **center** figure, it is clear to see that smaller  $\lambda_2$  on the fused graphical lasso penalty function shows better performance while in the **right** figure, larger  $\lambda_2$  on the group lasso penalty function achieves better performance.

For DGP1, we hypothesize that the fused graphical lasso would have the best performance in small sample size settings. This is because the fused graphical lasso encourages the similarity of both structure and values across groups. For DGP2, we expect that the group graphical lasso to have the best performance because it only encourages shared structure but allows flexibility for each group to retain different inverse covariance values. These two experiments demonstrate our hypothesis: if the joint models share the same inverse covariance values, the fused graphical lasso function has the largest AUC. On the other hand, if the joint models have a shared structure, but the structure has different inverse covariance values, the group graphical lasso has the largest AUC. Alternatively, we could select proper regularization functions based on prior knowledge about the form of the shared structures.

#### 7.3 Model Selection

To properly select the hyperparameters  $\lambda_1, \lambda_2$ , we employ the Bayesian Information Criterion (BIC) (Schwarz, 1978) as follows:

$$\lambda_1^*, \lambda_2^* = \underset{\lambda_1, \lambda_2}{\operatorname{argmin}} \sum_{k=1}^K tr(\widehat{\Sigma}^{(k)} \widehat{\Omega}^{(k)}) - \log\{\det(\widehat{\Omega}^{(k)})\} + E_k \log(n_k), \tag{15}$$

where  $\widehat{E}^{(k)}$  is the sampled covariance of group k,  $\widehat{\Omega}^{(k)}$  is the estimated precision matrix of group k,  $n_k$  is the number of samples of group k, and  $E_k$  is the number of nonzero elements of the precision matrix. The BIC method is a trade-off between the goodness of fit and the model complexity. The first term in (15) maximizes the data likelihood, while the second term penalizes the model complexity by discouraging the number of connected edges. We perform a grid search and find  $\lambda_1^*$ ,  $\lambda_2^*$  that achieves the minimum BIC value. Figure 6 illustrates an example of the fused graphical lasso model selection on graphs generated by DGP2, where the setting is p = 100, n = 50,  $\rho = 0.1$ .

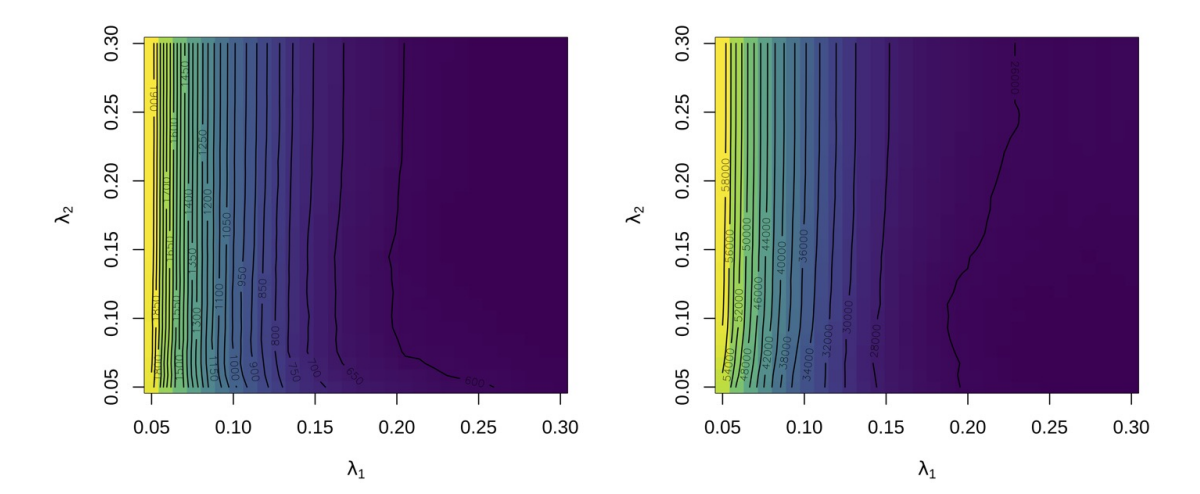


Figure 6: The **left** figure is the level sets of the BIC values with different  $\lambda_1$  and  $\lambda_2$ . The **right** figure is the AIC (Akaike, 1974) values with different  $\lambda_1$  and  $\lambda_2$ . The level lines are nearly vertical which indicate that tuning  $\lambda_1$  has more influence on the performance than tuning  $\lambda_2$  in our test settings.

### 7.4 Entropy Loss v.s. n/p

High-dimensional data is characterized by settings where n is much greater than p, leading to poor estimation results. This condition can be alleviated using regularizers. In this experiment, we evaluate the estimation performance with different regularizers when the ratio n/p is smaller than 1, meaning that we have more parameters than samples to estimate. We use the entropy loss (Guo et al., 2011) as an evaluation metric defined as:

$$EL = \frac{1}{K} \sum_{k=1}^{K} \text{tr}\{(\mathbf{\Omega}^{(k)})^{-1} \widehat{\mathbf{\Omega}}^{(k)}\} - \log|\det{\{\mathbf{\Omega}^{(k)}\}}^{-1} \widehat{\mathbf{\Omega}}^{(k)}\}| - p,$$

where k is the group index,  $\Omega^{(k)}$  is the ground truth precision matrix, and  $\widehat{\Omega}^{(k)}$  is the recovered precision matrix. Noting that the entropy loss here is equivalent to the Kullback-Leibler divergence of two centered multivariate Gaussian distributions, which is a widely used metric to evaluate the distance of two distributions. From the definition of entropy loss, it is clear that when  $\widehat{\Omega}^{(k)} = \Omega^{(k)}$  and the inverse of  $\Omega^{(k)}$  exist, the entropy loss reduces to 0.

In the following experiment, we test  $p = \{20, 50, 80, 100\}$  and change the number of samples n. The ground truth graphs are generated using DGP1 and each curve is the average of 5 replications. The model parameters are selected using BIC.

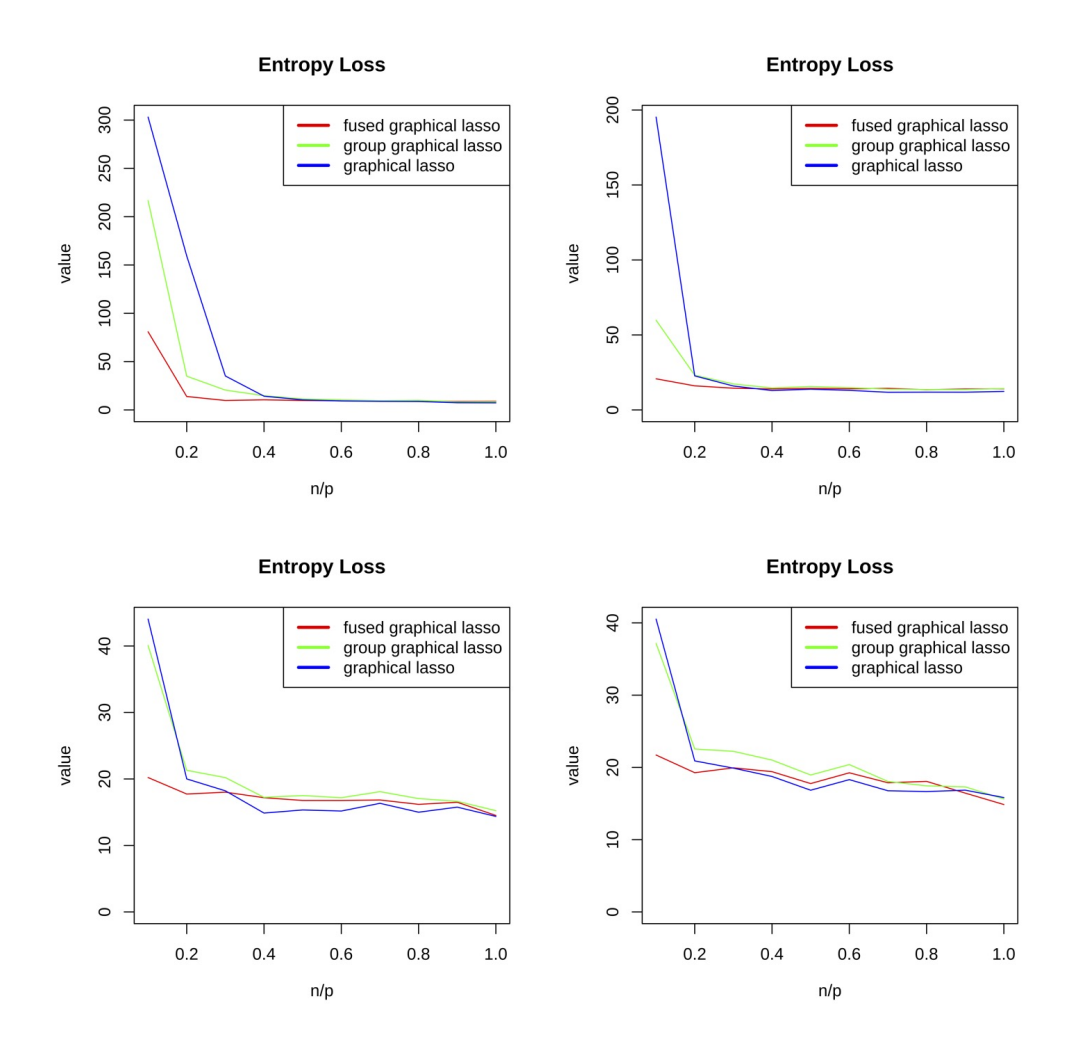


Figure 7: The **top left** figure shows when p = 20, **top right** figure shows when p = 50, **bottom left** figure shows when p = 80 and **bottom right** figure shows when p = 100. Among the four cases, when n/p is smaller than 0.2 the entropy curves have sharp slopes, and yet the fused graphical lasso method has the smallest slopes. This implies that under small sample size settings, joint estimation achieves better recovery. When the sample size n increases, the curves gradually become flat, and all three methods achieve comparable recovery performance.

### 7.5 Entropy Loss v.s. Graph Size

Now consider the case when the sample size n=10 is fixed, but the size of the graph is growing. We evaluate the performance of three penalty functions under this condition. In this experiment, we use DGP1 to construct the ground truth and the models are selected by BIC.

## **Entropy Loss** fused graphical lasso 80 group graphical lasso graphical lasso 9 value 40 20 0 2.0 2.2 1.4 1.6 1.8 log graph size

Figure 8: With the sample size fixed, the entropy loss increases as the graph size increases. The plot indicates that under this condition, the fused graphical lasso penalty function has a slower increase of the loss.

#### 7.6 Out-of-Sample Log-Likelihood

In most applications, we do not know the ground truth graph. Therefore, we cannot rely on the entropy loss or similar approach to evaluate the recovery. In this case, we split our data into training and test sets and use the test sets to evaluate the log-likelihood. We construct the ground truth using graph generation process 2 with K = 5, p = 100, n = 50 and the models are selected using BIC.

	fused graphical lasso	group graphical lasso	graphical lasso
$\lambda_1$	0.88	0.13	0.92
$\lambda_2$	0.01	1.0	
out-of-sample log-likelihood	-498.94	-489.99	-573.34

Table 2: Out-of-sample log-likelihood

# 8 Open Problems

Existing and emerging biological data and applications will require novel approaches to joint graphical models. We discuss some of these emerging applications briefly. Joint estimation of functional connectivity networks across multiple subjects allow scaling of the effective sample size and computation of estimates that are more robust to outliers. The joint estimators of brain connectivity networks could be applied to task-based fMRI scans to study group dynamic functional connectivity patterns (Andersen et al., 2018; Calhoun et al., 2014; Gonzalez-Castillo and Bandettini, 2018). While this manuscript is focused on joint estimation with the same set of nodes, one potential direction is to extend it to multiple sources, i.e., multimodal data. Recent technologies (Huster et al., 2012; Abreu et al., 2018) have demonstrated the availability of conducting concurrent measurements of EEG and fMRI signals, allowing the estimation of multiple sources possible in the future. While EEG has higher temporal resolution and fMRI features higher spatial resolution, we believe that joint estimation with multiple sources could compensate for the limits of the measurement techniques and provide better estimation results. Some recent work (Lock et al., 2013; Li and Li, 2021) has developed

methodologies to integrate data from different modalities, however, joint estimation of graphical models from multimodal data is still an open problem.

Approaches for the estimation of the joint graphical models presented in this survey largely rely on penalized estimation, where the penalty biases the estimates towards the assumed structure. Quantifying statistical uncertainty about the model parameters, that is, performing hypothesis tests and constructing confidence intervals, is challenging when penalized estimators are used due to the induced bias and model selection that is implicitly performed. There has been recent work on statistical inference for low-dimensional parameters in graphical models (Ren et al., 2015; Janková and van de Geer, 2015; Janková and van de Geer, 2017; Barber and Kolar, 2018; Wang and Kolar, 2016; Yu et al., 2016, 2020) based on the  $\ell_1$ -penalized estimator in the first stage. However, these approaches were developed only in the setting where parameters of one graph are being inferred. In contrast, work on statistical inference for joint graphical models is much more sparse. Xia et al. (2015); Belilovsky et al. (2016); Liu (2017); Kim et al. developed techniques for statistical inference in differential graphical models, while Wang and Kolar (2014); Lu et al. (2018); Wang et al. (2020a) focused on graphical models for time series data. Developing corresponding inferential techniques for estimators obtained using coarse-grained and fine-grained penalties is an interesting area open for future research.

### 9 Conclusion

This manuscript has introduced joint Gaussian graphical model estimation methods for joint data with shared structure across multiple groups. In particular, we consider several examples of extending classical statistical inference methods to joint estimation settings, including the MLE based estimator, neighborhood regression, and the CLIME estimator. We discuss several methods that exploit coarse-grained structures using a global regularization method that encourages shared coarse-grained structure across all groups. In contrast, the fine-grained structural regularization methods further partition the groups into subgroups per node, encouraging local shared regularity. With two groups, differential graphs are often a highly effective approach. The presented simulation experiments demonstrate that joint estimation can often recover the graphs more effectively than separate estimation for high dimensional data. Furthermore, we verify the characteristics of fused graphical lasso and group graphical regularizers for two data generation processes. When the data generation process has a shared inverse covariance structure with different values, group graphical lasso methods may be more effective. On the other hand, when the data generation process features a shared inverse covariance structure with the same values, the fused graphical lasso penalty function may perform better.

# **Funding Information**

O.Koyejo acknowledges partial funding from a C3.ai Digital Transformation Institute Award, a Jump Arches Award, and an Strategic Research Initiatives award from the University of Illinois at Urbana-Champaign. K.Tsai acknowledges funding from National Science Foundation Graduate Research Fellowships Program. Other authors have no relevant financial or non-financial interests to disclose. This work was also funded in part by the following grants: NSF III 2046795 and IIS 1909577, along with computational resources donated by Microsoft Azure.

# Further Reading

Recent developments of joint statistical inference are primarily focused on Gaussian graphical models. Other types of graphical models, including discrete graphical models (Drton and Richardson, 2008; Drton, 2009), semiparametric/nonparametric graphical models (Liu et al., 2012; Sun et al., 2015), and latent graphical models (Chandrasekaran et al., 2012), have been well studied for single graph estimation. While such models have broad applications, joint estimation in these models is less studied. A number of open source provided tools are available for joint estimation of multiple graphical models – Danaher et al. (2014); Li

et al. (2019); Bilgrau et al. (2020) have released an R-package for regularization-based methods; Lin et al. (2017) provide the MATLAB source code for the joint temporal and spatial estimation; Mohan et al. (2014) provides code for estimating differential graphs.

### References

- R. Abreu, A. Leal, and P. Figueiredo. Eeg-informed fmri: a review of data analysis methods. *Frontiers in human neuroscience*, 12:29, 2018.
- H. Akaike. A new look at the statistical model identification. *IEEE transactions on automatic control*, 19 (6):716–723, 1974.
- M. R. Andersen, O. Winther, L. K. Hansen, R. Poldrack, and O. Koyejo. Bayesian structure learning for dynamic brain connectivity. In 21st International Conference on Artificial Intelligence and Statistics, AISTATS 2018, pages 1436–1446, 2018.
- A. Atay-Kayis and H. Massam. A monte carlo method for computing the marginal likelihood in nondecomposable gaussian graphical models. *Biometrika*, 92(2):317–335, 2005.
- R. F. Barber and M. Kolar. Rocket: Robust confidence intervals via kendall's tau for transelliptical graphical models. *Ann. Statist.*, 46(6B):3422–3450, 2018.
- E. Belilovsky, G. Varoquaux, and M. B. Blaschko. Testing for differences in gaussian graphical models: Applications to brain connectivity. In D. D. Lee, M. Sugiyama, U. V. Luxburg, I. Guyon, and R. Garnett, editors, Advances in Neural Information Processing Systems 29, pages 595–603. Curran Associates, Inc., 2016.
- A. E. Bilgrau, C. F. Peeters, P. S. Eriksen, M. Bøgsted, and W. N. van Wieringen. Targeted fused ridge estimation of inverse covariance matrices from multiple high-dimensional data classes. *Journal of Machine Learning Research*, 21(26):1–52, 2020.
- P. Bühlmann and S. Van De Geer. Statistics for high-dimensional data: methods, theory and applications. Springer Science & Business Media, 2011.
- T. Cai, W. Liu, and X. Luo. A constrained  $\ell_1$  minimization approach to sparse precision matrix estimation. Journal of the American Statistical Association, 106(494):594–607, 2011.
- V. D. Calhoun, R. Miller, G. Pearlson, and T. Adalı. The chronnectome: time-varying connectivity networks as the next frontier in fmri data discovery. *Neuron*, 84(2):262–274, 2014.
- T. E. Chan, M. P. Stumpf, and A. C. Babtie. Gene regulatory network inference from single-cell data using multivariate information measures. *Cell systems*, 5(3):251–267, 2017.
- V. Chandrasekaran, P. A. Parrilo, and A. S. Willsky. Latent variable graphical model selection via convex optimization. The Annals of Statistics, 40(4):1935–1967, 2012.
- H. Chun, X. Zhang, and H. Zhao. Gene regulation network inference with joint sparse gaussian graphical models. Journal of Computational and Graphical Statistics, 24(4):954–974, 2015.
- G. L. Colclough, M. W. Woolrich, S. J. Harrison, P. A. R. López, P. A. Valdes-Sosa, and S. M. Smith. Multi-subject hierarchical inverse covariance modelling improves estimation of functional brain networks. *NeuroImage*, 178:370–384, 2018.
- P. Danaher, P. Wang, and D. M. Witten. The joint graphical lasso for inverse covariance estimation across multiple classes. *Journal of the Royal Statistical Society: Series B (Statistical Methodology)*, 76(2):373–397, 2014.
- A. Dobra, C. Hans, B. Jones, J. R. Nevins, G. Yao, and M. West. Sparse graphical models for exploring gene expression data. *Journal of Multivariate Analysis*, 90(1):196–212, 2004.
- F. Dondelinger, S. Lèbre, and D. Husmeier. Non-homogeneous dynamic bayesian networks with bayesian regularization for inferring gene regulatory networks with gradually time-varying structure. *Machine Learning*, 90(2):191–230, 2013.

- M. Drton. Discrete chain graph models. Bernoulli, 15(3):736-753, 2009.
- M. Drton and M. H. Maathuis. Structure learning in graphical modeling. Annual Review of Statistics and Its Application, 4(1):365–393, 2017.
- M. Drton and T. S. Richardson. Binary models for marginal independence. *Journal of the Royal Statistical Society: Series B (Statistical Methodology)*, 70(2):287–309, 2008.
- J. Felsenstein. Evolutionary trees from dna sequences: a maximum likelihood approach. *Journal of molecular evolution*, 17(6):368–376, 1981.
- N. J. Foti and E. B. Fox. Statistical model-based approaches for functional connectivity analysis of neuroimaging data. *Current opinion in neurobiology*, 55:48–54, 2019.
- N. Friedman, M. Linial, I. Nachman, and D. Pe'er. Using bayesian networks to analyze expression data. Journal of computational biology, 7(3-4):601–620, 2000.
- A. J. Gibberd and J. D. Nelson. Regularized estimation of piecewise constant gaussian graphical models: The group-fused graphical lasso. *Journal of Computational and Graphical Statistics*, 26(3):623–634, 2017.
- J. Gonzalez-Castillo and P. A. Bandettini. Task-based dynamic functional connectivity: Recent findings and open questions. Neuroimage, 180:526–533, 2018.
- K. Greenewald, S. Park, S. Zhou, and A. Giessing. Time-dependent spatially varying graphical models, with application to brain fmri data analysis. In *Advances in Neural Information Processing Systems*, pages 5832–5840, 2017.
- J. Guo, E. Levina, G. Michailidis, and J. Zhu. Joint estimation of multiple graphical models. Biometrika, 98(1):1–15, 2011.
- D. Hallac, Y. Park, S. Boyd, and J. Leskovec. Network inference via the time-varying graphical lasso. In Proceedings of the 23rd ACM SIGKDD International Conference on Knowledge Discovery and Data Mining, pages 205–213, 2017.
- B. Hao, W. W. Sun, Y. Liu, and G. Cheng. Simultaneous clustering and estimation of heterogeneous graphical models. *Journal of Machine Learning Research*, 18:217–1, 2018.
- C.-J. Hsieh, M. A. Sustik, I. S. Dhillon, P. K. Ravikumar, and R. Poldrack. Big & quic: Sparse inverse covariance estimation for a million variables. In *Advances in neural information processing systems*, pages 3165–3173, 2013.
- R. J. Huster, S. Debener, T. Eichele, and C. S. Herrmann. Methods for simultaneous eeg-fmri: an introductory review. *Journal of Neuroscience*, 32(18):6053–6060, 2012.
- J. Janková and S. van de Geer. Confidence intervals for high-dimensional inverse covariance estimation. Electron. J. Stat., 9(1):1205–1229, 2015.
- J. Janková and S. A. van de Geer. Honest confidence regions and optimality in high-dimensional precision matrix estimation. TEST, 26(1):143–162, 2017.
- B. Kim, S. Liu, and M. Kolar. Two-sample inference for high-dimensional markov networks. *Journal of the Royal Statistical Society: Series B (Statistical Methodology)*, n/a(n/a), arXiv:https://rss.onlinelibrary.wiley.com/doi/pdf/10.1111/rssb.12446.
- T. Kling, P. Johansson, J. Sanchez, V. D. Marinescu, R. Jörnsten, and S. Nelander. Efficient exploration of pan-cancer networks by generalized covariance selection and interactive web content. *Nucleic acids* research, 43(15):e98–e98, 2015.
- M. Kolar and E. P. Xing. Estimating networks with jumps. Electronic journal of statistics, 6:2069, 2012.

- M. Kolar, L. Song, A. Ahmed, E. P. Xing, et al. Estimating time-varying networks. *The Annals of Applied Statistics*, 4(1):94–123, 2010.
- S. L. Lauritzen. Graphical models, volume 17. Clarendon Press, 1996.
- W. Lee and Y. Liu. Joint estimation of multiple precision matrices with common structures. *The Journal of Machine Learning Research*, 16(1):1035–1062, 2015.
- A. Lenkoski and A. Dobra. Computational aspects related to inference in gaussian graphical models with the g-wishart prior. *Journal of Computational and Graphical Statistics*, 20(1):140–157, 2011.
- Q. Li and L. Li. Integrative factor regression and its inference for multimodal data analysis. *Journal of the American Statistical Association*, pages 1–15, 2021.
- Z. Li, T. Mccormick, and S. Clark. Bayesian joint spike-and-slab graphical lasso. In *International Conference on Machine Learning*, pages 3877–3885. PMLR, 2019.
- Z. Lin, T. Wang, C. Yang, and H. Zhao. On joint estimation of gaussian graphical models for spatial and temporal data. *Biometrics*, 73(3):769, 2017.
- H. Liu, F. Han, M. Yuan, J. Lafferty, and L. Wasserman. High-dimensional semiparametric gaussian copula graphical models. *The Annals of Statistics*, 40(4):2293–2326, 2012.
- W. Liu. Structural similarity and difference testing on multiple sparse Gaussian graphical models. Ann. Statist., 45(6):2680–2707, 2017.
- E. F. Lock, K. A. Hoadley, J. S. Marron, and A. B. Nobel. Joint and individual variation explained (jive) for integrated analysis of multiple data types. *The annals of applied statistics*, 7(1):523, 2013.
- J. Lu, M. Kolar, and H. Liu. Post-regularization inference for time-varying nonparanormal graphical models. Journal of Machine Learning Research, 18(203):1–78, 2018.
- J. Lukemire, S. Kundu, G. Pagnoni, and Y. Guo. Bayesian joint modeling of multiple brain functional networks. *Journal of the American Statistical Association*, pages 1–13, 2020.
- J. Ma and G. Michailidis. Joint structural estimation of multiple graphical models. *The Journal of Machine Learning Research*, 17(1):5777–5824, 2016.
- M. Maathuis, M. Drton, S. Lauritzen, and M. Wainwright. Handbook of graphical models. CRC Press, 2018.
- S. Majumdar and G. Michailidis. Joint estimation and inference for data integration problems based on multiple multi-layered gaussian graphical models. arXiv preprint arXiv:1803.03348, 2018.
- J. R. Manning, X. Zhu, T. L. Willke, R. Ranganath, K. Stachenfeld, U. Hasson, D. M. Blei, and K. A. Norman. A probabilistic approach to discovering dynamic full-brain functional connectivity patterns. NeuroImage, 180:243-252, 2018.
- B. M. Marlin and K. P. Murphy. Sparse gaussian graphical models with unknown block structure. In *Proceedings of the 26th Annual International Conference on Machine Learning*, pages 705–712, 2009.
- N. Meinshausen, P. Bühlmann, et al. High-dimensional graphs and variable selection with the lasso. *The annals of statistics*, 34(3):1436–1462, 2006.
- T. J. Mitchell and J. J. Beauchamp. Bayesian variable selection in linear regression. *Journal of the american statistical association*, 83(404):1023–1032, 1988.
- R. Mitra, P. Müller, Y. Ji, et al. Bayesian graphical models for differential pathways. *Bayesian Analysis*, 11 (1):99–124, 2016.
- A. Mohammadi, E. C. Wit, et al. Bayesian structure learning in sparse gaussian graphical models. *Bayesian Analysis*, 10(1):109–138, 2015.

- K. Mohan, M. Chung, S. Han, D. Witten, S.-I. Lee, and M. Fazel. Structured learning of gaussian graphical models. In *Advances in neural information processing systems*, pages 620–628, 2012.
- K. Mohan, P. London, M. Fazel, D. Witten, and S.-I. Lee. Node-based learning of multiple gaussian graphical models. *The Journal of Machine Learning Research*, 15(1):445–488, 2014.
- R. P. Monti, P. Hellyer, D. Sharp, R. Leech, C. Anagnostopoulos, and G. Montana. Estimating time-varying brain connectivity networks from functional mri time series. *NeuroImage*, 103:427–443, 2014.
- S. Na, M. Kolar, and O. Koyejo. Estimating differential latent variable graphical models with applications to brain connectivity. *Biometrika*, 108(2):425–442, 2021.
- C. Peterson, F. C. Stingo, and M. Vannucci. Bayesian inference of multiple gaussian graphical models. Journal of the American Statistical Association, 110(509):159–174, 2015.
- E. Pierson, D. Koller, A. Battle, S. Mostafavi, G. Consortium, et al. Sharing and specificity of co-expression networks across 35 human tissues. *PLoS computational biology*, 11(5):e1004220, 2015.
- R. A. Poldrack, J. A. Mumford, and T. E. Nichols. *Handbook of functional MRI data analysis*. Cambridge University Press, 2011.
- B. S. Price, A. J. Molstad, and B. Sherwood. Estimating multiple precision matrices with cluster fusion regularization. *Journal of Computational and Graphical Statistics*, pages 1–12, 2021.
- H. Qiu, F. Han, H. Liu, and B. Caffo. Joint estimation of multiple graphical models from high dimensional time series. *Journal of the Royal Statistical Society: Series B (Statistical Methodology)*, 78(2):487–504, 2016.
- Z. Ren, T. Sun, C.-H. Zhang, and H. H. Zhou. Asymptotic normality and optimalities in estimation of large Gaussian graphical models. *Ann. Stat.*, 43(3):991–1026, 2015.
- A. Roverato. Hyper inverse wishart distribution for non-decomposable graphs and its application to bayesian inference for gaussian graphical models. *Scandinavian Journal of Statistics*, 29(3):391–411, 2002.
- T. Saegusa and A. Shojaie. Joint estimation of precision matrices in heterogeneous populations. *Electronic journal of statistics*, 10(1):1341, 2016.
- J. Schäfer and K. Strimmer. A shrinkage approach to large-scale covariance matrix estimation and implications for functional genomics. Statistical applications in genetics and molecular biology, 4(1), 2005.
- S. Schwab, R. Harbord, V. Zerbi, L. Elliott, S. Afyouni, J. Q. Smith, M. W. Woolrich, S. M. Smith, and T. E. Nichols. Directed functional connectivity using dynamic graphical models. *NeuroImage*, 175:340–353, 2018.
- G. Schwarz. Estimating the dimension of a model. The annals of statistics, pages 461–464, 1978.
- L. Shan and I. Kim. Joint estimation of multiple gaussian graphical models across unbalanced classes. Computational Statistics & Data Analysis, 121:89–103, 2018.
- L. Shan, Z. Qiao, L. Cheng, and I. Kim. Joint estimation of the two-level gaussian graphical models across multiple classes. *Journal of Computational and Graphical Statistics*, 29(3):562–579, 2020.
- J. M. Shine, P. G. Bissett, P. T. Bell, O. Koyejo, J. H. Balsters, K. J. Gorgolewski, C. A. Moodie, and R. A. Poldrack. The dynamics of functional brain networks: integrated network states during cognitive task performance. *Neuron*, 92(2):544–554, 2016.
- A. Shojaie. Differential network analysis: A statistical perspective. Wiley Interdisciplinary Reviews: Computational Statistics, 13(2):e1508, 2021.
- A. Skripnikov and G. Michailidis. Regularized joint estimation of related vector autoregressive models. Computational Statistics & Data Analysis, 139:164 177, 2019.

- S. Sun, M. Kolar, and J. Xu. Learning structured densities via infinite dimensional exponential families. *Advances in neural information processing systems*, 28:2287–2295, 2015.
- L. S. Tan, A. Jasra, M. De Iorio, T. M. Ebbels, et al. Bayesian inference for multiple gaussian graphical models with application to metabolic association networks. *The Annals of Applied Statistics*, 11(4):2222–2251, 2017.
- H. Wang. Bayesian graphical lasso models and efficient posterior computation. *Bayesian Analysis*, 7(4): 867–886, 2012.
- J. Wang and M. Kolar. Inference for sparse conditional precision matrices. *ArXiv e-prints, arXiv:1412.7638*, 2014, arXiv:1412.7638.
- J. Wang and M. Kolar. Inference for high-dimensional exponential family graphical models. In A. Gretton and C. C. Robert, editors, Proceedings of the 19th International Conference on Artificial Intelligence and Statistics, volume 51 of Proceedings of Machine Learning Research, pages 1042–1050, Cadiz, Spain, 2016. PMLR.
- X. Wang, M. Kolar, and A. Shojaie. Statistical inference for networks of high-dimensional point processes. arXiv:2007.07448, 2020a, arXiv:2007.07448v1.
- Y. Wang, S. Segarra, and C. Uhler. High-dimensional joint estimation of multiple directed gaussian graphical models. *Electronic Journal of Statistics*, 14(1):2439–2483, 2020b.
- Y. Xia, T. Cai, and T. T. Cai. Testing differential networks with applications to the detection of gene-gene interactions. *Biometrika*, 102(2):247–266, 2015.
- P. Xu and Q. Gu. Semiparametric differential graph models. Advances in Neural Information Processing Systems, 29:1064–1072, 2016.
- M. Yajima, D. Telesca, Y. Ji, and P. Müller. Detecting differential patterns of interaction in molecular pathways. *Biostatistics*, 16(2):240–251, 2014.
- J. Yang and J. Peng. Estimating time-varying graphical models. Journal of Computational and Graphical Statistics, 29(1):191–202, 2020.
- M. Yu, V. Gupta, and M. Kolar. Statistical inference for pairwise graphical models using score matching. In *Advances in Neural Information Processing Systems 29*. Curran Associates, Inc., 2016.
- M. Yu, V. Gupta, and M. Kolar. Simultaneous inference for pairwise graphical models with generalized score matching. *Journal of Machine Learning Research*, 21(91):1–51, 2020.
- H. Yuan, R. Xi, C. Chen, and M. Deng. Differential network analysis via lasso penalized d-trace loss. *Biometrika*, 104(4):755–770, 2017.
- M. Yuan and Y. Lin. Model selection and estimation in the gaussian graphical model. *Biometrika*, 94(1): 19–35, 2007.
- B. Zhao, Y. S. Wang, and M. Kolar. Direct estimation of differential functional graphical models. *Advances in Neural Information Processing Systems*, 32:2575–2585, 2019.
- S. D. Zhao, T. T. Cai, and H. Li. Direct estimation of differential networks. *Biometrika*, 101(2):253–268, 2014.
- S. Zhou, J. D. Lafferty, and L. A. Wasserman. Time varying undirected graphs. *Mach. Learn.*, 80(2-3): 295–319, 2010a.
- S. Zhou, J. Lafferty, and L. Wasserman. Time varying undirected graphs. *Machine Learning*, 80(2):295–319, 2010b.
- Y. Zhu and O. Koyejo. Clustered fused graphical lasso. In UAI, pages 487–496, 2018.